Suspended Sediment Sampling and Annual Sediment Yield on the Middle Trinity River

University of Houston, Houston, Texas

PI: Kyle Strom, Associate Professor
Civil and Environmental Engineering

Submitted To: Texas Water Development Board
Research Project: 1248311361
Research Report: Final Report

January, 2015

Suspended Sediment Sampling and Annual Sediment Yield on the Middle Trinity River

Kyle Strom[1] and Hossein Hosseiny[2]

Final Report
Sponsor Research Project ID: 1248311361
Research Project Title:"Suspended Sediment Sampling and Annual Sediment Yield on the Middle Trinity River"
Sponsored by Texas Water Development Board

January, 2015

Department of Civil and Environmental Engineering
University of Houston
Houston, Texas 77204-4003

[1]Associate Professor, Civil and Environmental Engineering, Virginia Tech, Blacksburg, VA 24061-0105, phone: 540.231.0979, e-mail: strom@vt.edu. Formerly at the University of Houston.
[2]Graduate Research Assistant, Civil and Environmental Engineering, University of Houston.

Abstract

This report presents measured sediment transport data and an effective discharge analysis for four USGS gage stations along the Trinity River between Rosser, TX and Crockett, TX. Measurements of channel cross-sectional properties, bed sediment grain-size distribution, suspended sediment concentration, and the suspended sediment grain size distribution were made between January 1, 2012 to August 31, 2014 over a range of flow conditions. Sediment rating curves for suspended load (measured) and bed load (calculated) and SAMwin calculated total load were developed and used in combination with USGS measured flow rates and historic sediment data to facilitate the calculation of the effective discharge and the sediment half-load discharge at each station. Effective discharge was computed using two different methods for developing the pdf of the mean daily flow and using two different methods for obtaining the total bed material load; i.e., one using the rating curves for the measured suspended load and calculated bed load, and one using a simple Einstein total load equation to calculate both bed and suspended load in the software package SAMwin. The effective and half-load discharges are compared to the pure flow metrics of bankfull and the 1.5 year return period flow. The calculated effective discharge progressed in the downstream direction from approximately 11,000 cfs at Rosser to 20,000 cfs at Crockett. The half-load and effective discharges were approximately equivalent. It was also found that the effective discharge could be calculated at each of the sites using only the bed load rating curve, and that identical effective discharges could be calculated using SAMwin to generate the flow and sediment transport data using only the measured bed material grain size distribution and channel cross sectional properties. The effective and half-load discharges were on the same order, but lower in magnitude, than the 1.5 year return period and bankfull discharges. The 1.5 year return period flow was nearly constant for all four stations. Whereas, the bankfull flow increase from station to station in the downstream direction. Yearly sediment yields of bed load and suspended bed material load are reported for each station using the USGS flow data from January 1, 1990 to December 31, 20013 and the computed rating curves for each transport mode and station.

Disclaimer

The contents of this report reflect the views of the author(s), who is (are) responsible for the facts and the accuracy of the data presented herein. The contents do not necessarily reflect the official view or policies of Texas Water Development Board. This report does not constitute a standard, specification, or regulation. This report is not intended for construction, bidding, or permit purposes. Trade or manufacturers names appear herein solely because they are considered essential to the object of this report. The researcher in charge of the project was Dr. Kyle Strom.

Acknowledgements

Kyle Strom and Hossein Hosseiny would like to acknowledge and thank Nolan Raphelt and Mark Wentzel of the TWDB for their cooperation, guidance, and support of the project. We would also like to thank the following graduate and undergraduate students for their help with sample collection and processing: Mohamad Rouhnia, Duc Tran, Frederick Ma, and Jose Mendiola.

Contents

List of Figures

List of Tables

1 Introduction

1.1 Project goal and objectives

The goal of the project was to develop annual sediment yield and effective discharge estimates for four gaging stations along the Trinity River from the USGS gaging station near Rosser, TX down to the station near Crocket, TX. The work was performed in cooperation with the Instream Flow Team of the Texas Water Development Board (TWDB) and focused on obtaining field measurements of sediment transport at each gaging site over a range of flow conditions. The collected data was then used as to developing annual sediment yield and effective discharge estimates at each station. The specific objectives of the project were to:

1. Develop sediment rating curves based on field measurements for the following four USGS gaging stations.

   (a) 08062500 - Trinity River near Rosser, TX

   (b) 08062700 - Trinity River at Trinidad, TX

   (c) 08065000 - Trinity River near Oakwood, TX

   (d) 08065350 - Trinity River near Crockett, TX

2. Integrate the sediment rating curves with the annual flow duration curves to produce annual sediment yield histograms and the effective discharges at each of the four gaging stations.

3. Present the work in a written report, scientific journal, and technical conference.

1.2 Overview of approach

Sediment rating curves are site-specific relations that give sediment daily discharge as a function of daily water discharge at a particular river location. The site-specific nature of such relations requires that field measurements of sediment discharge be made over a range of flow conditions, at the location of interest, for the development of the rating curves. Obtaining this data can be difficult and time intensive. This project focuses on collecting suspended sediment samples over a range of flow conditions at each of the four gaging sites listed under objective 1. Collecting bedload samples was out of the scope of this project. Instead, bedload was estimated at each station using measured cross sectional data, sampled bed material, and bedload discharge relations. The measured suspended sediment load is used to develop the rating curves which give suspended sediment load in tons per day as a function of mean daily flow. The rating curves are then used along with the calculated bedload and the flow frequency histograms developed from USGS data at each gage to produce sediment yield histograms from which the effective discharge for each station is determined (objective 2); the effective discharge is defined as the mean of the discharge increment that transports the largest fraction of the annual

sediment load over a period of 20 years (from January 1, 1990, to December 31, 2012). Sediment yield is then computed for each station by year using the historic daily mean flow data and the developed rating curves (objective 2). This report summarizes the methods, data, and results of the study (objective 3).

1.3 Study sites

The four gaging station sites along the Trinity are shown below in figures 1.1 through 1.3.

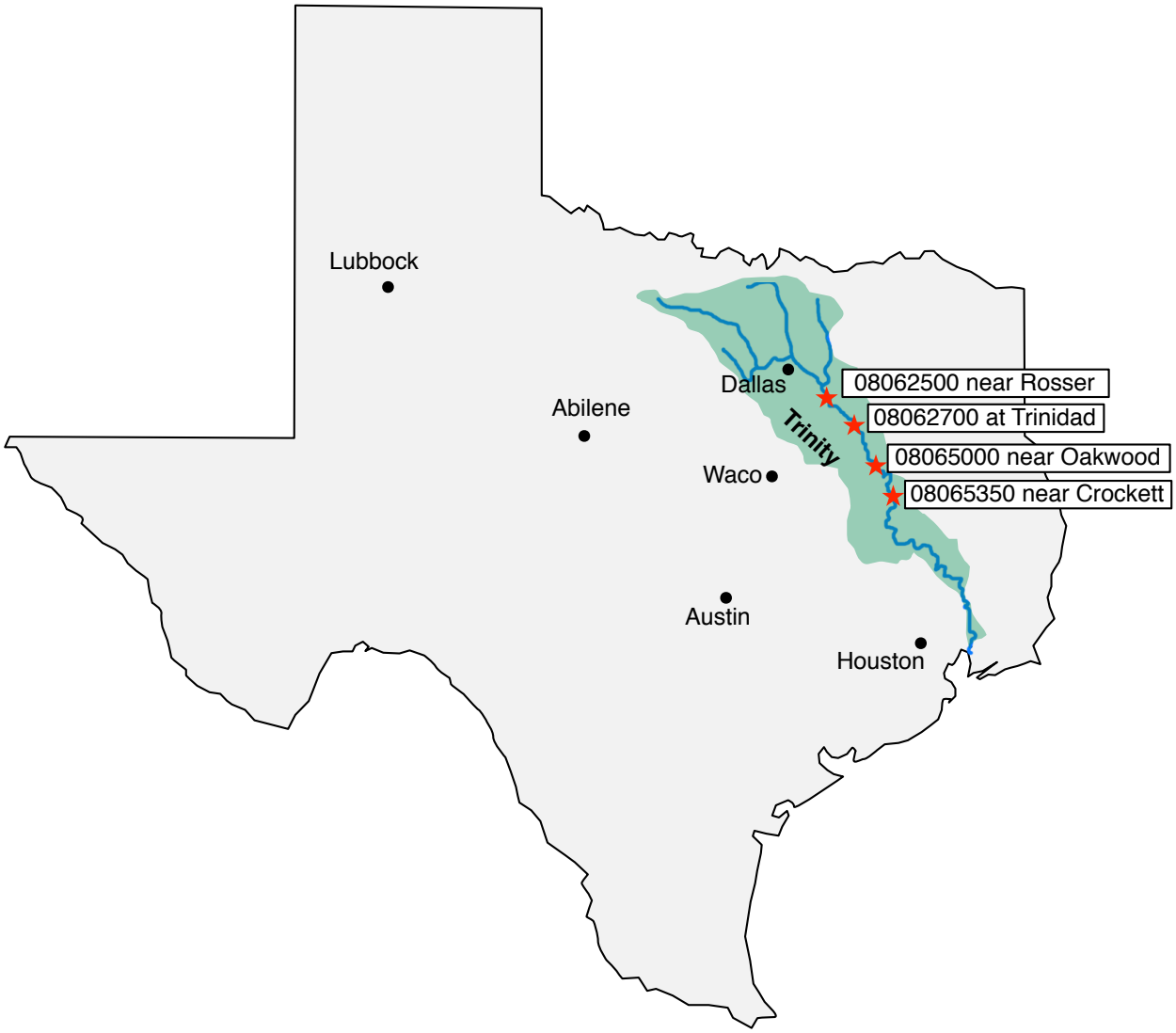

Figure 1.1: A map of Texas showing the Trinity watershed and the study gaging stations.

Figure 1.2: Pictures of the Trinity from each the study bridge near the gaging stations. (A-B) Rosser 08062500 (Google Map image), and (C-D) Trinidad 08062700 (Google Map image). All photos are taken at low flow conditions.

Figure 1.3: Pictures of the Trinity from each the study bridge near the gaging stations. (A-B) Oakwood 08065000, and (C-D) Crockett 08065350. All photos are taken at low flow conditions.

2 Background

2.1 Effective discharge

Rivers are dynamic entities that self organize in response to imposed tectonic and climatic forces. The concept of a river at "grade" formally put forward by Mackin (1948) is useful for helping to building a framework from which to understand the trajectory of a river with time in response to the imposed boundary conditions. The grade concept simply states that a river reach will modify its slope, through vertical aggradation or degradation and/or lateral change, in such a way as to transport all of the imposed sediment at a given water discharge. This idea was built upon by Lane (1955) who parameterized the concept of a stream at grade as having,

$$QS \propto Q_S d \tag{2.1}$$

where Q is a characteristic dominant volumetric water discharge, S is the channel slope at grade, Q_S is the total bed material sediment load (bed load + suspended load), and d is the characteristic sediment grain size. While the Lane relationship is not dimensionally homogenous, and clearly a simplification, it can be useful for framing the long-term response of a river to boundary conditions changes. For example, if slope increased due to tectonic uplift, then either or both the sediment load and/or size would need to increase at the given water discharge to produce a stream at an equilibrium grade. Or, if sediment load increases but discharge stays constant, the stream would respond by steepening its slope with time (Fig. 2.1). In the transition from one equilibrium state to another, a channel will adjust to the new conditions until the channel comes into a new dynamic equilibrium about the graded state where, on average, there is neither net degradation or aggradation in the channel, i.e., the same volume of sediment leaves the reach as enters it. (Fig. 2.1).

Inherent in the concept of a graded river and the Lane formulation is the notion that the river is responding to some characteristic channel-forming discharge, and that the river itself is alluvial and free to deform its boundaries through erosion of past deposits or deposition of current sediment loads. While a river can be conceptualized as morphologically responding to

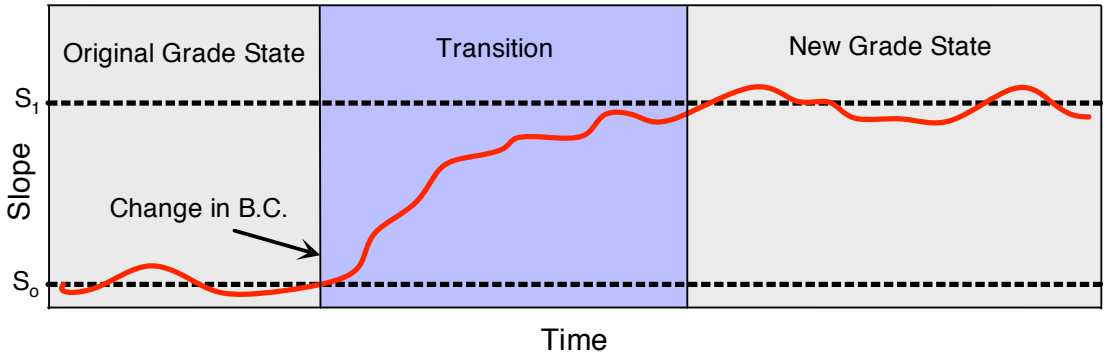

Figure 2.1: Schematic example of a channel adjusting its slope from S_o to S_1 in response to a change in bed material load, Q_b.

some characteristic constant discharge, the discharge in natural rivers continually varies over a range of flow conditions, and one is faced with the question of, "what is the dominant channel-forming discharge that the river is morphologically responding to?" This dominant discharge is typically taken to be either the bankfull flow or the effective discharge. The bankfull flow is the discharge that just fills the channel to its banks (identified by a slope break in the stage discharge curve), and the effective discharge is defined as the discharge which moves the greatest percentage of bed material in a river over a given period of time (Wolman and Miller, 1960; Biedenharn et al., 2000). Another way to think about the effective discharge concepts is as, the discharge that does the most geomorphic work or the discharge that has the most "geomorphic effectiveness" (Wolman and Miller, 1960). Often these two characteristic discharges (bankfull and effective) are fairly close in magnitude and often have return periods on the order of 1 to 2 years (Andrews, 1980; Whiting et al., 1999; Emmett and Wolman, 2001), though they do not necessarily have to be similar (e.g., Pickup and Warner, 1976). Another measure of the dominant discharge of a river is the half-load discharge, $Q_{1/2}$, of Vogel et al. (2003), which is defined as the flow above and below which one half of the total bed material load is transported over a given time period. The half-load discharge is typically associated with a higher magnitude and longer return period flow than the effective discharge (Vogel et al., 2003; Klonsky and Vogel, 2011).

2.2 Calculating effective discharge

Various methods have been used to calculate the conceptualized effective discharge (Wolman and Miller, 1960; Sichingabula, 1999; Crowder and Knapp, 2005; Lenzi et al., 2006; Klonsky and Vogel, 2011). The most often used method is the one proposed by Wolman and Miller (1960), where the probability density function (pdf) or histogram of the daily mean flow is multiplied by the average sediment load to produce a histogram of sediment loads, $S_h = S_h(Q)$, that represents the fraction of load carried by a given discharge, Q, over the time interval of interest,

$$S_h = Q_s f_Q \tag{2.2}$$

where, $Q_s = Q_s(Q)$ is the daily sediment load (in tons per day) associated with the daily discharge value of Q, and f_Q is the pdf of the daily flow discharges (percent of time that the flow was at a rate of Q). Q_s is the total sediment bed material load and includes contributions from both bed load, Q_b, and suspended load Q_{sbm}. Sediment load histograms of the form of S_h (equation 2.2) can be developed for suspended and bed material load independently and then added together for determination of the effective discharge (Andrews, 1980; Biedenharn et al., 2000), or they can be based solely on suspended material if the transport mode is suspension dominated (Wolman and Miller, 1960; Sichingabula, 1999); often times, the analysis is done using only the suspended load because suspended load is typically the only data easily available (e.g., Klonsky and Vogel, 2011). Typically, in developing the sediment load histogram, S_L, a rating curve that gives the average sediment load as a function of discharge, $Q_s = Q_s(Q)$, is developed from historic or measured data using regression. The sediment load rating curve take the form of:

$$Q_s = \alpha Q^{\beta} \tag{2.3}$$

where α and β are site-specific coefficients that can be obtained through regression of the Q_s and Q paired data. Once α and β are obtained, the sediment rating equation can be used with

the pdf of the daily flow data to produce a histogram that shows the distribution of the percentage of total sediment load as a function of flow rate following equation 2.2 (fig. 2.2). The effective discharge is then selected as the flow rate, Q, associated with the peak in the S_h histogram.

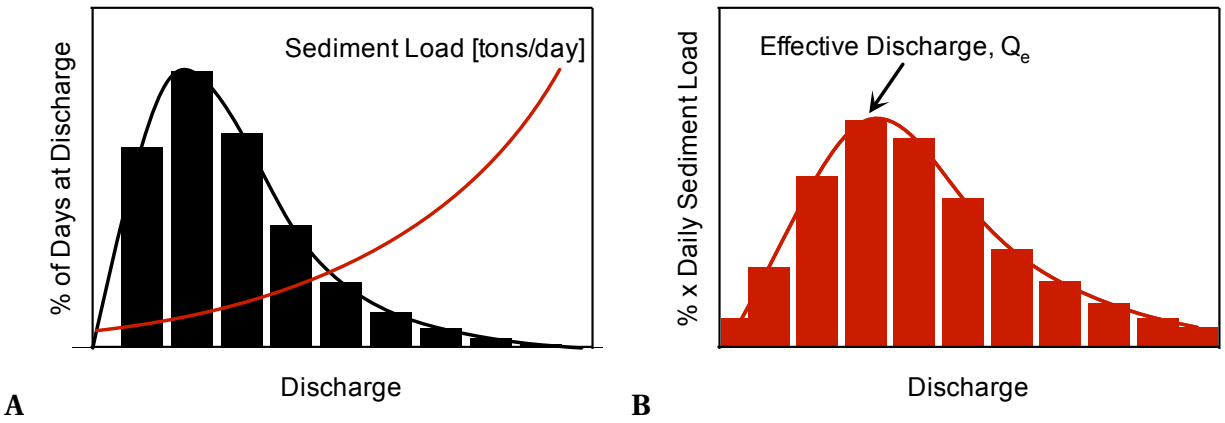

Figure 2.2: Example of a flow duration histogram (A) and a sediment load histogram (B).

Practically, f_Q is typically constructed as discrete histogram and not a continuous function. When this is the case, the discharge values used in equation 2.2 are those associated with the mid point of each discharge histogram bin (fig. 2.2A), and the effective discharge, Q_e, is the discharge of the mid point of the bin associated with the peak of the histogram.

2.3 Methods for constructing the PDF of the daily flow data

One of the biggest sources of variability in the calculation of the effective discharge comes through the way in which the pdf of the daily flow data, f_Q (also known as the flow frequency and flow duration histogram) is produced (Sichingabula, 1999; Biedenharn et al., 2000; Crowder and Knapp, 2005; Lenzi et al., 2006; Ma et al., 2010; Klonsky and Vogel, 2011). The flow frequency distribution is produced using historical measurements of the discharge over a substantial amount of time (10 or more years if possible); the discharges can be 15-minute, 1-hour, or mean daily data. The discharges are then binned and the percentage in each bin is calculated to create f_Q. Typically, the width of the bins is set manually, and some adjustment to the bin widths may be required to keep the peak in the sediment discharge histogram from occurring in the first bin (Biedenharn et al., 2000). Manual selection of the bin width is based on past experience and some general guidelines such as, starting out by sorting the flow into 25 arithmetically even-spaced bins (Hey, 1997; Biedenharn et al., 2000) and then adjusting bin number/width as needed. In the end, the exact bin number/width used is the result of trial and error, where the bin numbers are iteratively adjusted until a relatively smooth rising and falling of the sediment histogram has been developed. Developing a representative histogram or pdf of the discharge is a key since the shape of the curve, which is determined by bin number/width selection and the historical data, greatly influences the calculation of effective discharge.

Because the effective discharge calculation is dependent on the way in which the pdf of the flow data is built, methods have been sought to remove a degree of subjectiveness in cre-

ation of the flow frequency distribution. One of the more prominent methods does this through use of the kernel density function (Klonsky and Vogel, 2011). The kernel density function is non-parametric way to estimate the pdf of a random variable, in this case the mean daily discharge over a range of time. In their study, Klonsky and Vogel (2011) demonstrated that the kernel density function was a viable method for objectively evaluating both the effective and half-load discharges.

For calculating the effective discharge on the Trinity, this study uses both the traditional method of manually selecting the width of the discharge bins for the development of the flow frequency histogram and the non-parametric kernel disunity function of Klonsky and Vogel (2011).

3 Methods

3.1 Data needed

The effective discharge and annual sediment yield calculations require (1) historic discharge data for development of the daily flow pdf and (2) sediment load data for the development of sediment rating curves for each gaging station (eq. 2.3). Q_s in equation 2.3 is defined as the total bed material load, which is equal to the bed material load moving in suspension plus the bed material load moving in contact with the bed region, i.e. the bed load. Development of sediment rating curves for each station was done using physical measurements of the suspended sediment load and calculation of the bed load using bed load equations and measured cross sectional properties of the channel similar to that of Andrews (1980) and Biedenharn et al. (2000). Therefore, data needed to define Q_s at a given flow rate included: measurement of the cross-sectionally averaged suspended sediment concentration, measurement of the grain size distribution of the sediment in suspension, measurement of the channel cross-sectional geometry and cross-sectional flow area, the bed material grain size distribution, the reach slope, and the flow discharge.

3.2 Flow conditions and historic flow statistics

The data needed was collected at six different flow conditions covering a range of high, moderate, and low flow conditions at each of the six sites. The relative magnitude of high, moderate, and low flow at each site were based on exceedance values of historic, daily-mean discharge data obtained from the USGS National Water Information System (NWIS) from January 1, 1990 to December 31, 2012. For the study, high, moderate, and low flow were defined as follows: a high flow is a discharge that has historically been exceeded less than 20 percent of the time; moderate flow is a discharge that has historically been exceeded between 20 and 50 percent of the time; and low flow is a discharge that has historically been exceeded between 50 to 90 percent of the time. Of the six measurements planned per gaging site, two were made at high flow conditions, two at moderate flow conditions, and two at low flow conditions (table 3.1). The specific discharge values at the cuts of 90, 50, and 20 percent of the time exceeded for each of the four sites can be found in Table 3.2.

Sites	# of Samples	Relative Flow Magnitude	Flow Exceedance Condition
All 4 sites	2	High	Q exceeded $\leq 20\%$
All 4 sites	2	Moderate	$20\% \leq Q$ exceeded $\leq 50\%$
All 4 sites	2	Low	$50\% \leq Q$ exceeded $\leq 90\%$

Table 3.1: Sampling conditions. Six measurements per station.

Station	gage #	20 Years of Record						All Years of Record		
		Exceedance Values			Return Periods			Return Periods		
		$Q_{90\%}$ [cfs]	$Q_{50\%}$ [cfs]	$Q_{20\%}$ [cfs]	$Q_{1.5}$ [cfs]	Q_2 [cfs]	Q_{10} [cfs]	$Q_{1.5}$ [cfs]	Q_2 [cfs]	Q_{10} [cfs]
Rosser	8062500	800	1500	7000	29543	34100	78774	20800	26000	58600
Trinidad	8062700	800	1600	8500	26600	37250	66974	25650	32600	68004
Oakwood	8065000	900	2200	11200	28200	44052	94770	22500	36100	90191
Crockett	8065350	1000	2500	13600	30100	38700	93348	25700	32800	69000

Table 3.2: Discharge statistics for the percent of time exceeded ($Q_{90\%}$, $Q_{50\%}$, and $Q_{20\%}$) along with the 1.5, 2, and 10 year return period flows calculated by ranking and linear interpolation using available USGS data for the 20 year analysis time period and using all available data.

3.3 Monitoring and predicting flow conditions

Obtaining enough lead time to get out and sample the suspended sediment at the gaging stations was an important element of the project. To help with this, some simple guidelines were developed to keep track of current conditions and predict likely flow conditions at each of the stations. The simple guidelines were based on monitoring of the realtime data coming from the USGS gaging stations and monitoring of the predicted and measured rainfall over the lower watershed.

Capturing high discharges at the Rosser stations was the most difficult due to the distance from Houston to the station. Downstream of Rosser, historic data at the four gages were used to estimate the amount of time required for a flood peak to travel between each gage. While the exact time it takes for a flood wave to pass from one gaging site to another changes as a function of rain fall location and intensity, the values obtained from this analysis did provide some helpful guidelines about the timing and attenuation of the flood wave as it passed through the system. This information, along with daily monitoring of the flow rates at the USGS gage stations and monitoring of the National Weather Service predicted and measured rainfall over the lower watershed was used to plan sampling trips.

3.4 Data collection methods

All four of the gage sites are located at bridge crossing. Accessibility to the bridge decks for sampling purposes varies with location. Some stations only required closure of the shoulder, while others required full lane closures. All lane closures were conduced by N-LINE Traffic Maintenance. For sites that only needed shoulder closures, the appropriate signs, barricades, and cones were used to protect field personnel following Traffic Control Plans (TCP) (1-1b)-98 as specified by the Texas Department of Transportation.

The primary data collected during each sampling trip included: a cross-sectionally integrated water column sample for measurement of the suspended sediment concentration, a cross sectionally integrated water column sample for measurement of the grain size distribution of the material in suspension, a bed material sample for characterization of the bed material size distribution, and measurement of the river boundary at the cross section.

The water column samples used for determination of the suspended sediment concentration and grain size distribution were obtained using a bucket on a rope, and a Federal Interagency Sedimentation Project (FISP) depth-integrated sampler (US DH-2TM bag-type) and the Equivalent Width Increment (EWI) method (Diplas et al., 2008). The US DH-2TM bag-type sampler is designed to collect 1 L isokinetic samples in depths up to 35 ft and velocities in the range of 2.0 to 6.0 ft/sec. The sampler was lowered and raised using a three-wheel truck USGS Type A crane with a B-56M sounding reel (fig. 3.1A). Nozzles of differing inner diameter (3/16", 1/4", and 5/16") were used to optimize the sampler for the flow conditions present at the time of sample collection, while keeping the sampler transit rate through the vertical limited to 40% of the mean channel velocity (Edwards and Glysson, 1999; Davis, 2005). All water samples from individual vertical transits were combined to create a integrated samples for the cross section following the EWI method. In general, velocities on the Trinity were too slow during the "low" flow conditions for use of the depth-integrated sampler. When deployed during these periods of low velocity, the sampler simply would not fill with water. Therefore, for the low flow conditions, data from the bucket sampler were used. Interestingly, for all flow conditions sampled with both methods, it was found that both the concentration and suspended grain size distribution were approximately equivalent.

Figure 3.1: Primary sampling equipment. (A) US DH-2TM bag-type sampler suspended from the sampling crane; (B) US BMH-60 bed material sampler; and (C) sounding weight.

A US BMH-60 FISP scoop-type bed material sampler suspended from the sampling crane (fig. 3.1B) was used to collect samples of the bed material at each measurement increment across the channel width. All samples were combined in a bucket to provide a single representative bed material sample for the cross section. Cross sectional data was obtained using a sounding weight dropped from the bridge deck using the sampling crane (fig. 3.1C). At each increment across the width, the distance to the bed and water surface from the bridge railing was recored. For consistency, the sampling increments across the bridge were setup from the same starting point on each repeated visit. During most of the high flow conditions, drag on the sounding weight and bed material sampler as they passed down through the water column was great enough to prevent data from being obtained with the sounding weight and bed material sampler.

Field samples of suspended sediment were processed in the laboratory to obtain average the suspended sediment concentration, C, associated with each particular flow discharge. Measurements of the total suspended sediment concentration was obtained through filtering for the lower concentration sample following the ASTM standards outlined in ASTM D3977 -

97(2007) (ASTM, 2007). For higher concentrations, the entire water and sediment mixture was placed in pre-weighed pans. The pans were then placed in an oven at low temperatures to evaporate all of the water and dry the sediment out. Following several days in the oven, the pans were reweighed to allow for calculation of the total suspended sediment mass. Bed material samples were sieved to produce a percent finer than by weight grain size distribution. The grain size distribution of the sediment in suspension was measured by running small, well-mixed water column samplers through a Malvern Mastersizer capable of measuring particle sizes in the range of 0.05 μm to 0.9 mm.

4 Data

4.1 Summary of flow conditions captured

This project officially ran from January 1, 2012 to August 31, 2014 and samples were collected throughout the duration of the project. In total, 23 of the planned 24 measurements were collected. One high flow sample at Rosser was not collected due to difficulty in getting to the station in time to capture the peak flow. The largest flow event to occur during the sampling period took place during the last week of November 2013. However, while the discharge during this event still did not reach the 1.5 year return period flow for any of the stations (table 3.2). Suspended sediment measurements were captured during the rising limb of this event at Crockett and on the falling limb at Oakwood.

4.2 Notes on measured data

Summary figures of the collected data are shown below figures 4.1-4.4, and all collected data is listed in table 4.1. Discharges shown in the figures and tables are the 15-minute USGS instantaneous discharges. The actual discharge at the time of measurement was typically slightly different than the mean daily value. However, we use the mean daily discharge throughout since the effective discharge calculations are based on mean daily data.

Two types of concentrations and suspended sediment discharges are reported. The first is the total suspended sediment load, Q_{ss} [tons/day], which contains both suspended bed material and suspended wash load; suspended bed material was defined as material coarser than 0.062 mm. Q_{ss} is calculated using the total concentration measurement from the sampler multiplied by the volume of flow passing the station in one day,

$$Q_{ss} = (1.1 \times 10^{-6}) C_{ss} V_{24\text{hr}} \tag{4.1}$$

where C_{ss} is the concentration in g/m^3 (which is equivalent to the concentration in mg/l), $V_{24\text{hr}}$ is the volume of water in m^3 passing the station per day, and 1.1×10^{-6} is a factor used to convert from grams to US short tons so that the units on Q_{ss} work out to be tons/day. The second type of suspended sediment load shown in the figures and tables and used in the analysis is the suspended bed material load, Q_{sbm}, computed as,

$$Q_{sbm} = \left(\frac{100 - \%WL}{100} \right) Q_{ss} \tag{4.2}$$

where, $\%WL$ is the wash load percentage, defined as the percent by volume of the material traveling in suspension that is less than 0.062 mm. $\%WL$ was calculated using the Malvern measured suspended sediment grain size distributions. For sampling dates without Malvern measurements of the suspended sediment, $\%WL$ values for flows that most closely matched the missing data were used (table 4.1).

In general, suspended sediment discharge increased with stream discharge. However, for some cases, the largest measured total suspended concentrations (bed material + wash load)

occurred at moderate discharges. For example, at Oakwood, the maximum measured suspended sediment concentration was 2.7 g/l and this was associated with a moderate discharge of 5,010 cfs on 5/18/13. Comparatively, concentrations were 1.1 g/l during the time of measurement on 10/31/13 when flows reached 18,100 cfs (table 4.1). Such differences are likely reflective of sampling variability or differences in wash load produced by variations in location of rainfall, vegetation cover, or land use. Maximum observed suspended sediment concentrations per site are marked in table 4.1 with bold text, and the maximum daily discharge for the sampling days is highlighted with italics. Bolded italics are used when the two maximums coincide. This occurred at Rosser and Crockett (table 4.1).

An unusual occurrence in the dataset for the suspended sediment is that the overall largest grain size distributions for each site were associated with low and moderate flow events. While no strong trend in size was present with discharge, suspended sediment samples taken during the high flow conditions did consistently produce some of the finest observed suspended sediment grain size distributions (figures 4.1-4.4).

Channel cross sectional geometry measurements are expected to be the most accurate during the low flow conditions. During high flow, it is possible that drag on the sounding weight made the cross section appear to be "deeper" than it actually was due to the angled line-of-fall of the weight. Therefore, all cross sectional data presented was collected at low or the lower end of the moderate flow condition. Some data was collected during higher flows, but this data is not presented because of the significant drag observed on the sounding weight.

Figure 4.5 shows the overall downstream trends for drainage area, slope (discussed in detail in the next section), active channel width, bankfull depth, return period flows at 1.5, 2, and 10 years, and the average bed material grain size statistics. As expected, channel width and depth both slightly increase in the downstream direction. Also, on average, discharge increases and grain size decreases moving down from Rosser to Crockett.

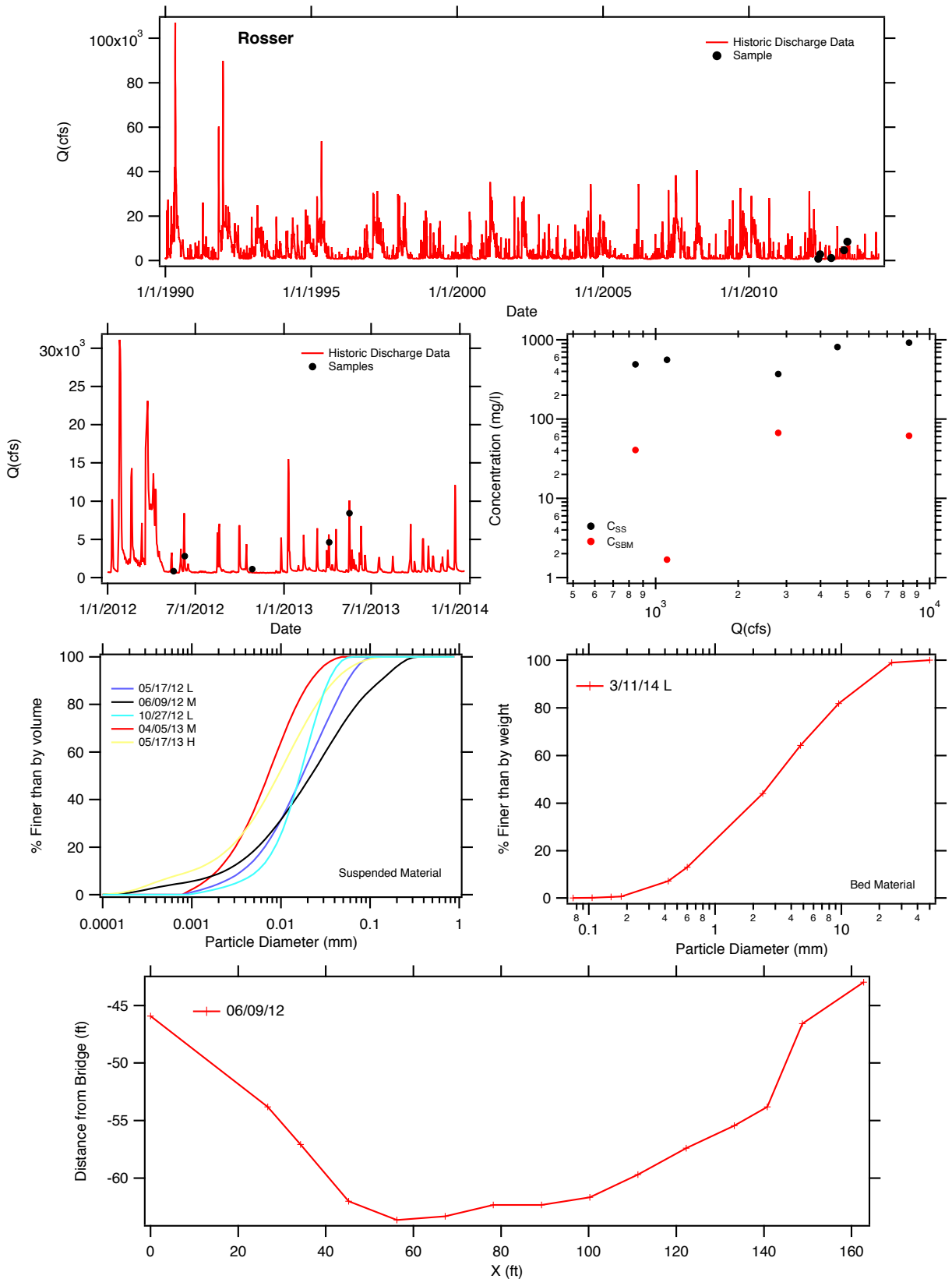

Figure 4.1: Summary of collected data at Rosser (USGS gage 08062500).

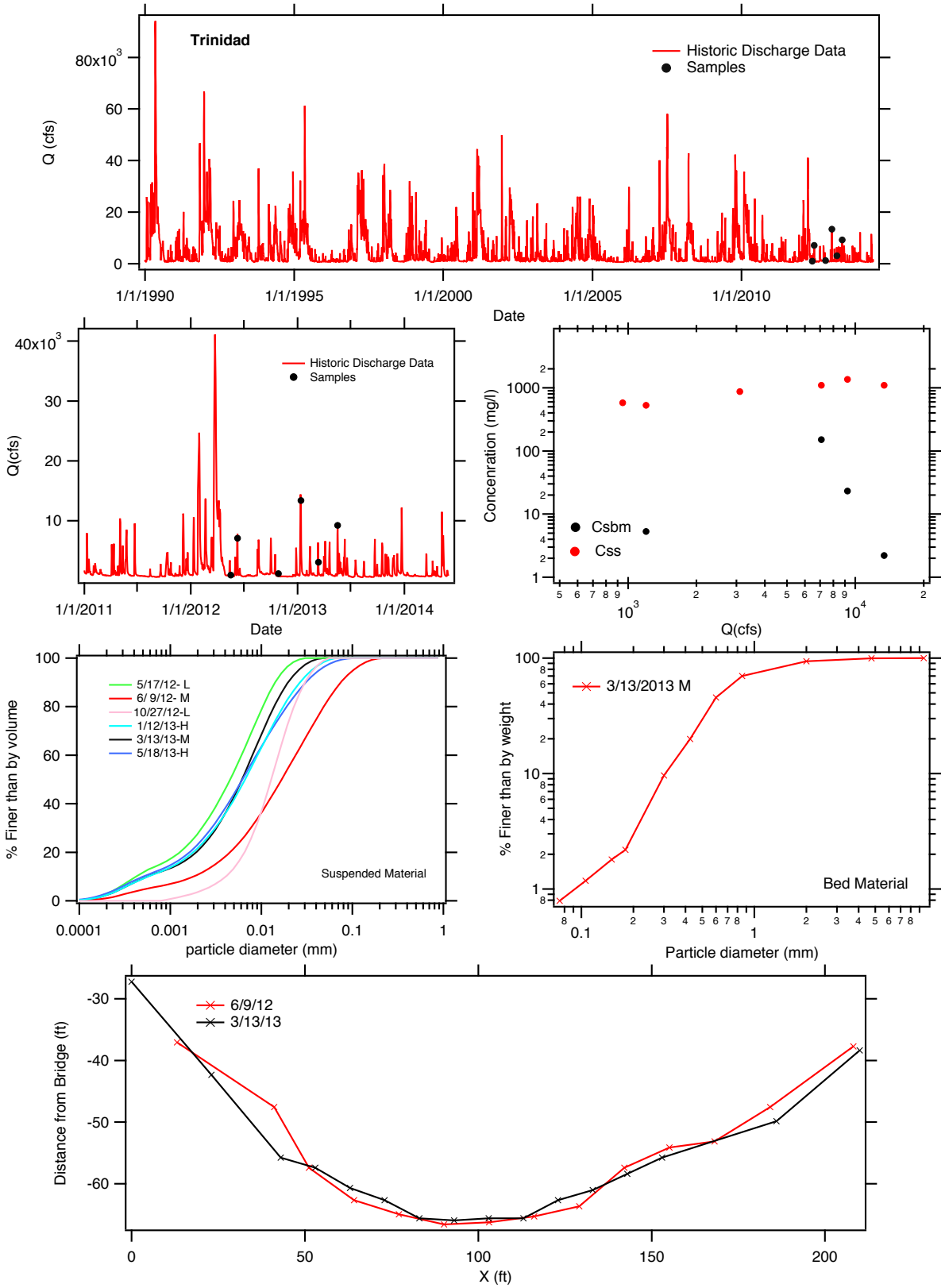

Figure 4.2: Summary of collected data at Trinidad (USGS gage 08062700).

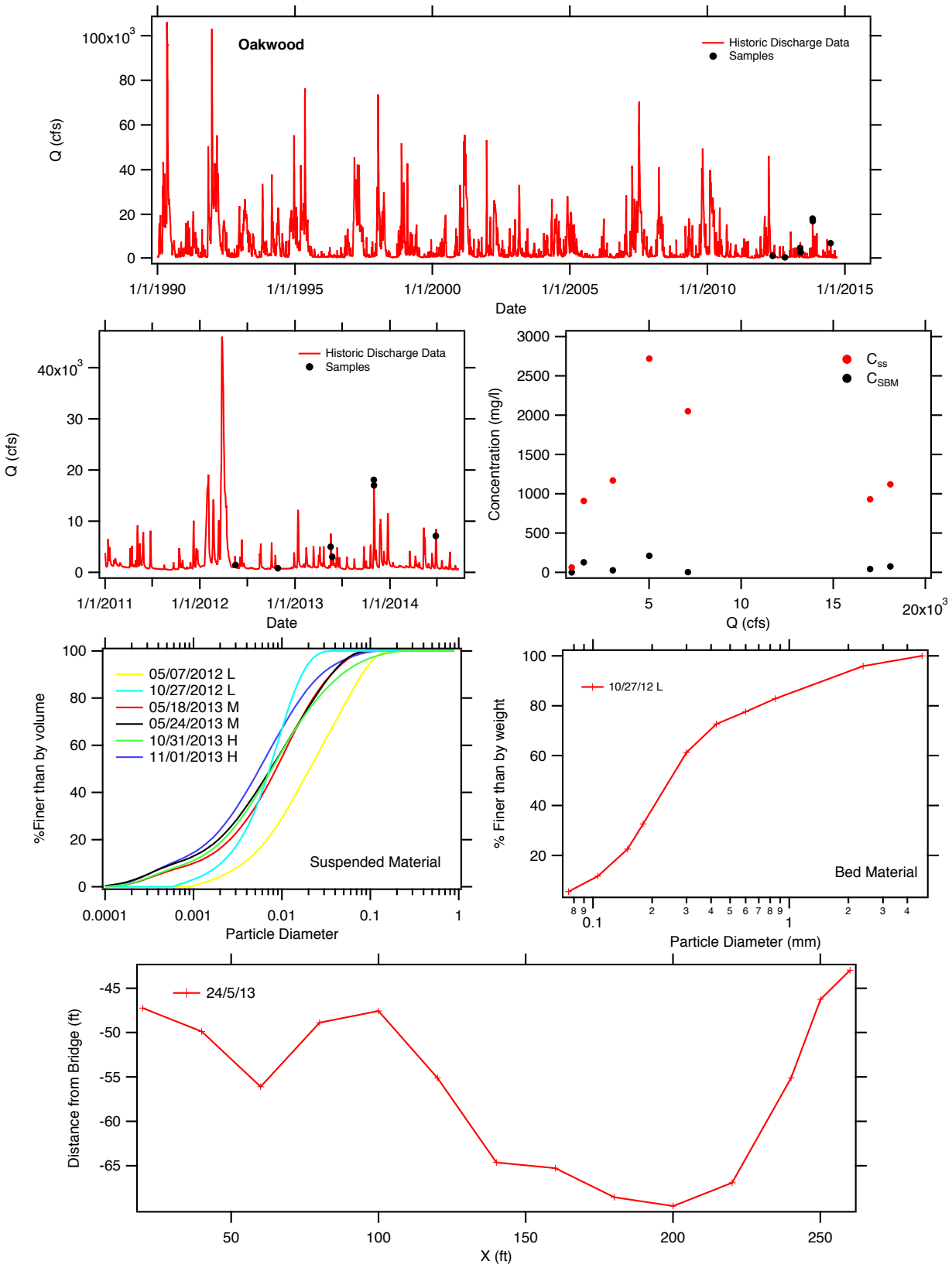

Figure 4.3: Summary of collected data at Oakwood (USGS gage 08065000).

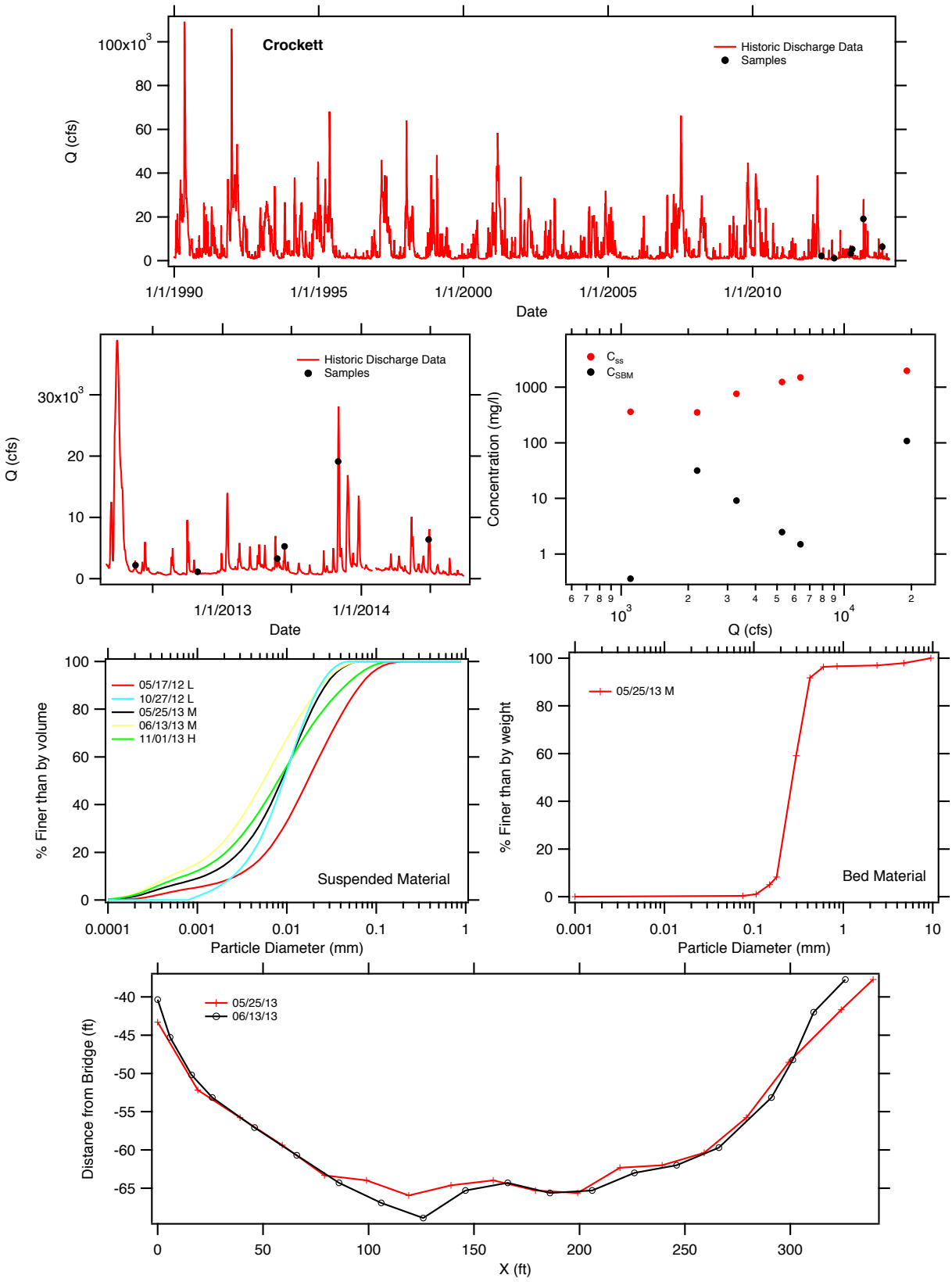

Figure 4.4: Summary of collected data at Crockett (USGS gage 08065350).

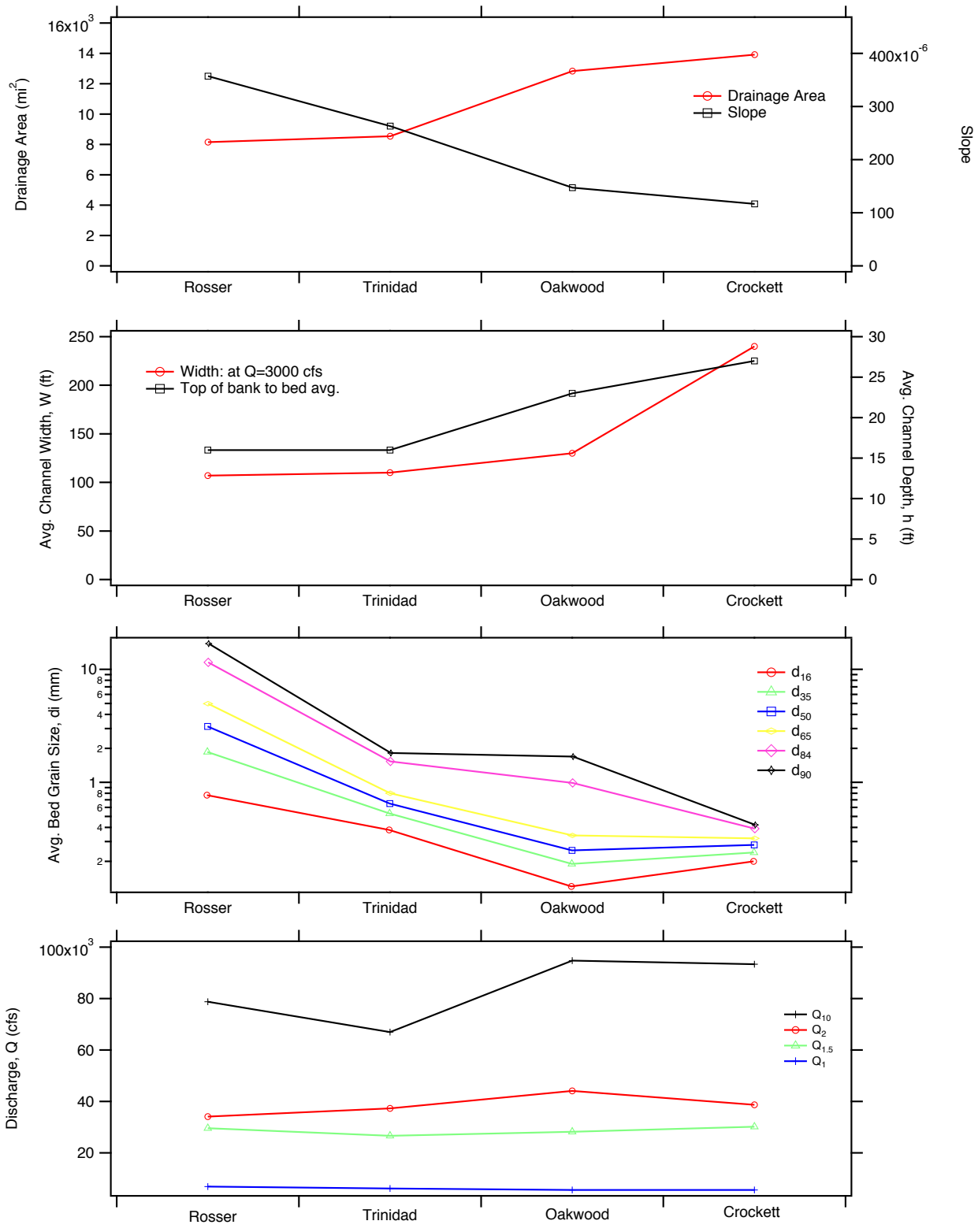

Figure 4.5: Downstream trends in major steam properties.

Site	Date	Condition	Location on Hydrograph	SS Sample Method	Bed Size Measured? (Used)	SS Size Measured? (Used)	Q [cfs]	R_h [ft]	U [ft/s]	Bed Material d_{16} [mm]	d_{50} [mm]	d_{84} [mm]	d_{90} [mm]	Wash Load [%]	Total SSC [mg/l]
Rosser	5/17/12	Low	Base	Bucket	No (3/11/14)	Yes	844	4.3	2	0.77	3.13	11.52	16.91	91.7	490
Rosser	6/9/12	Moderate	Falling	DIS	No (3/11/14)	Yes	2800	6.2	3.8	0.77	3.13	11.52	16.91	81.9	370
Rosser	10/27/12	Low	Base	Bucket	No (3/11/14)	Yes	1100	4.5	2.5	0.77	3.13	11.52	16.91	99.7	560
Rosser	4/5/13	Moderate	Falling	DIS	No (3/11/14)	Yes	4610	7.1	5.4	0.77	3.13	11.52	16.91	99.9	810
Rosser	5/17/13	High	Peak	DIS	No (3/11/14)	Yes	***8410***	11.2	5.3	0.77	3.13	11.52	16.91	93.3	**920**
Rosser	3/11/14	Low	Base	Bucket	Yes	No (5/7/12)	718	4.1	1.9	0.77	3.13	11.52	16.91	91.7	490
Trinidad	5/17/12	Low	Base	Bucket	No (3/13/13)	Yes	946	4.2	2.8	0.38	0.65	1.53	1.82	99.9	580
Trinidad	6/9/12	Moderate	Falling	DIS	No (3/13/13)	Yes	7080	10.5	4.1	0.38	0.65	1.53	1.82	86.3	1100
Trinidad	10/27/12	Low	Base	Bucket	No (3/13/13)	Yes	1200	4.8	2.9	0.38	0.65	1.53	1.82	99	530
Trinidad	1/12/13	High	Peak	DIS	No (3/13/13)	Yes	*13400*	14	4.3	0.38	0.65	1.53	1.82	99.8	1100
Trinidad	3/13/13	Moderate	Falling	DIS	Yes	Yes	3100	6	4.5	0.38	0.65	1.53	1.82	99.9	870
Trinidad	5/18/13	High	Peak	DIS	No (3/13/13)	Yes	**9240**	12.6	4.1	0.38	0.65	1.53	1.82	98.3	**1360**
Oakwood	5/17/12	Low	Falling	Bucket	No (10/27/12)	Yes	1460	7.5	1.7	0.12	0.25	0.99	1.69	86.1	910
Oakwood	10/27/12	Low	Base	Bucket	Yes	Yes	800	5.8	1.3	0.12	0.25	0.99	1.69	99.9	62
Oakwood	5/18/13	Moderate	Rising	DIS	No (10/27/12)	Yes	**5010**	11.6	3	0.12	0.25	0.99	1.69	92.2	**2720**
Oakwood	5/24/13	Moderate	Rising	DIS	No (10/27/12)	Yes	3030	9.4	2.6	0.12	0.25	0.99	1.69	97.7	1170
Oakwood	10/31/13	High	Rising	DIS	No (10/27/12)	Yes	*18100*	17.9	3.3	0.12	0.25	0.99	1.69	93.3	1119
Oakwood	11/1/13	High	Falling	DIS	No (10/27/12)	Yes	17000	17.1	3.3	0.12	0.25	0.99	1.69	95.5	930
Oakwood	6/27/14	Moderate	Rising	DIS	No (10/27/12)	Yes	7110	13.1	3.5	0.12	0.25	0.99	1.69	99.9	2050
Crcokett	5/17/12	Low	Falling	Bucket	No (5/25/13)	Yes	2190	7.4	1.1	0.2	0.28	0.39	0.42	91	350
Crcokett	10/27/12	Low	Base	Bucket	No (5/25/13)	Yes	1100	6.6	0.7	0.2	0.28	0.39	0.42	99.9	360
Crcokett	5/25/13	Moderate	Peak	DIS	Yes	Yes	3290	8	1.6	0.2	0.28	0.39	0.42	98.8	760
Crcokett	6/13/13	Moderate	Peak	DIS	No (5/25/13)	Yes	5260	8.8	2.2	0.2	0.28	0.39	0.42	99.8	1240
Crcokett	11/1/13	High	Rising	DIS	No (5/25/13)	Yes	***19100***	16.4	3.5	0.2	0.28	0.39	0.42	94.5	**1960**
Crcokett	6/27/14	Moderate	Rising	DIS	No (5/25/13)	Yes	6370	9.3	2.5	0.2	0.28	0.39	0.42	99.9	1500

Table 4.1: Summary of measured data. **Bolded** text highlights the highest measured concentrations at that site, and the *italics* highlights the highest daily main discharge during the sampling at the site. For the ***bolded italics***, the two maximums coincided.

4.3 Comparison of data to historic sources

The collected suspended and bed material samples were compared to USGS measured values when available from each of the four gage stations. The USGS dataset for these sites contains spot measurements between 1964 to 1994. The Rosser, Oakwood, and Crockett sites all contain measurements of total suspended sediment concentration, percent wash load, a limited suspended bed material grain size distribution, and bed material size distribution. At Trinidad, only data for total suspended sediment and the percentage of wash load are available. The USGS data for the sites was obtained from the NWIS sites for each gage under the "Water Quality: Field/Lab Sample" section.

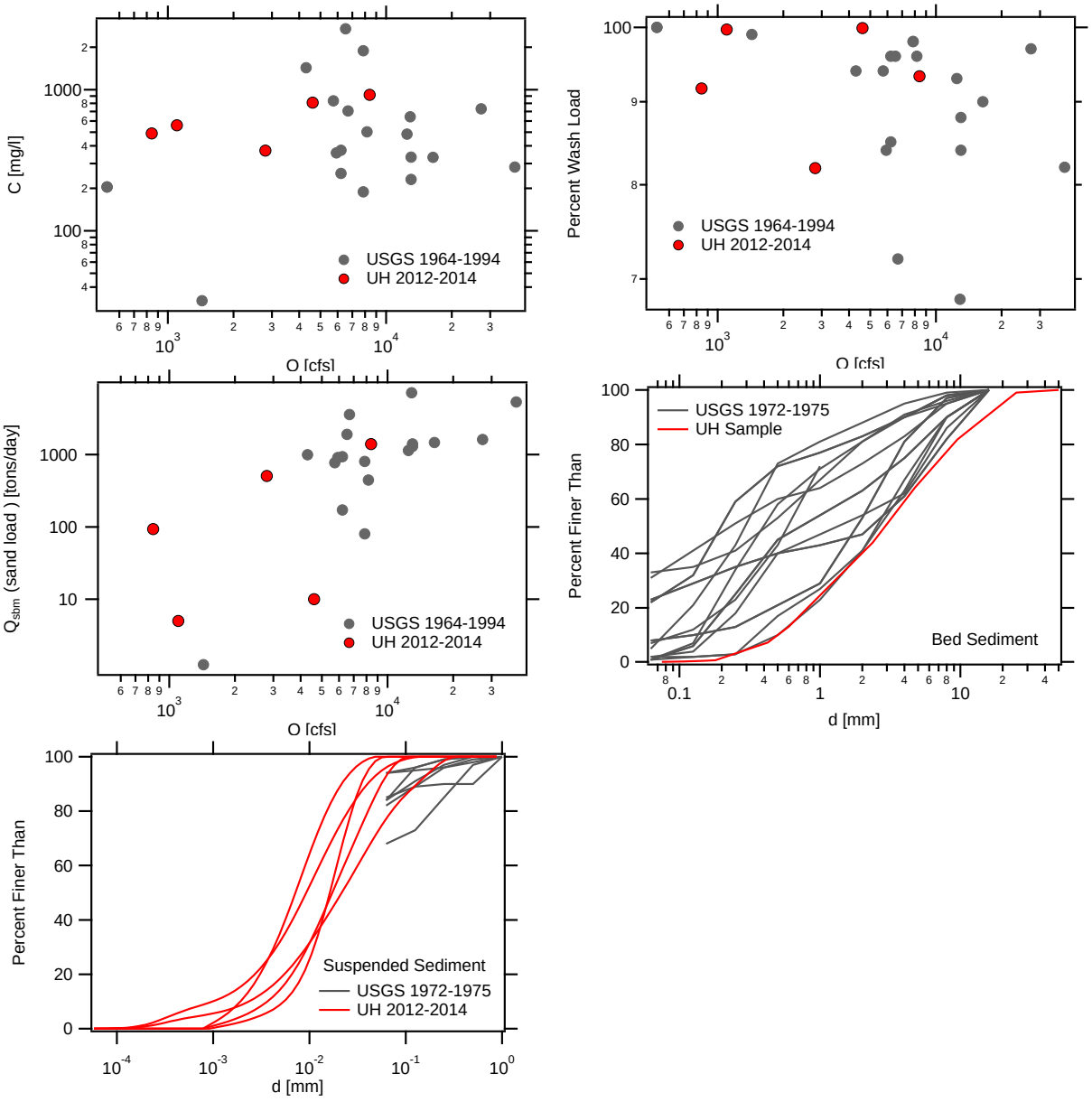

Figure 4.6: Comparison of UH and USGS data at the Rosser station.

Comparisons of the measured concentrations and suspended bed material load with the historic data shows that the newly measured total concentrations fall within the range of those previously observed, but that they are, in general, a bit higher than most of the the historic values. This is especially true for the Trinidad and Crockett sites (figures 4.7 and 4.9). However, the measured sand loads from all sites between the UH measurements and the USGS measurements are very comparable for all sites. The newly measured bed material grain size distribution are all comparable to the older USGS values (figures 4.6, 4.8, 4.9).

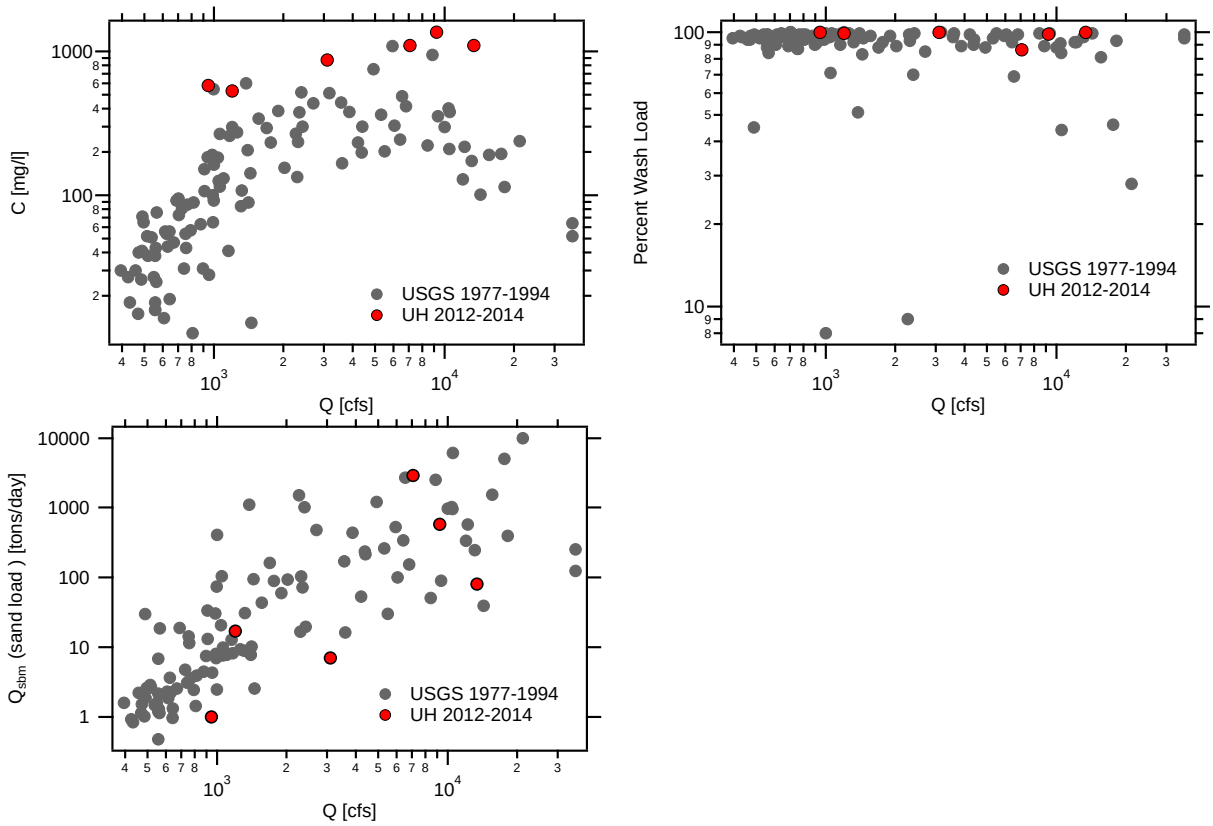

Figure 4.7: Comparison of UH and USGS data at the Trinidad station.

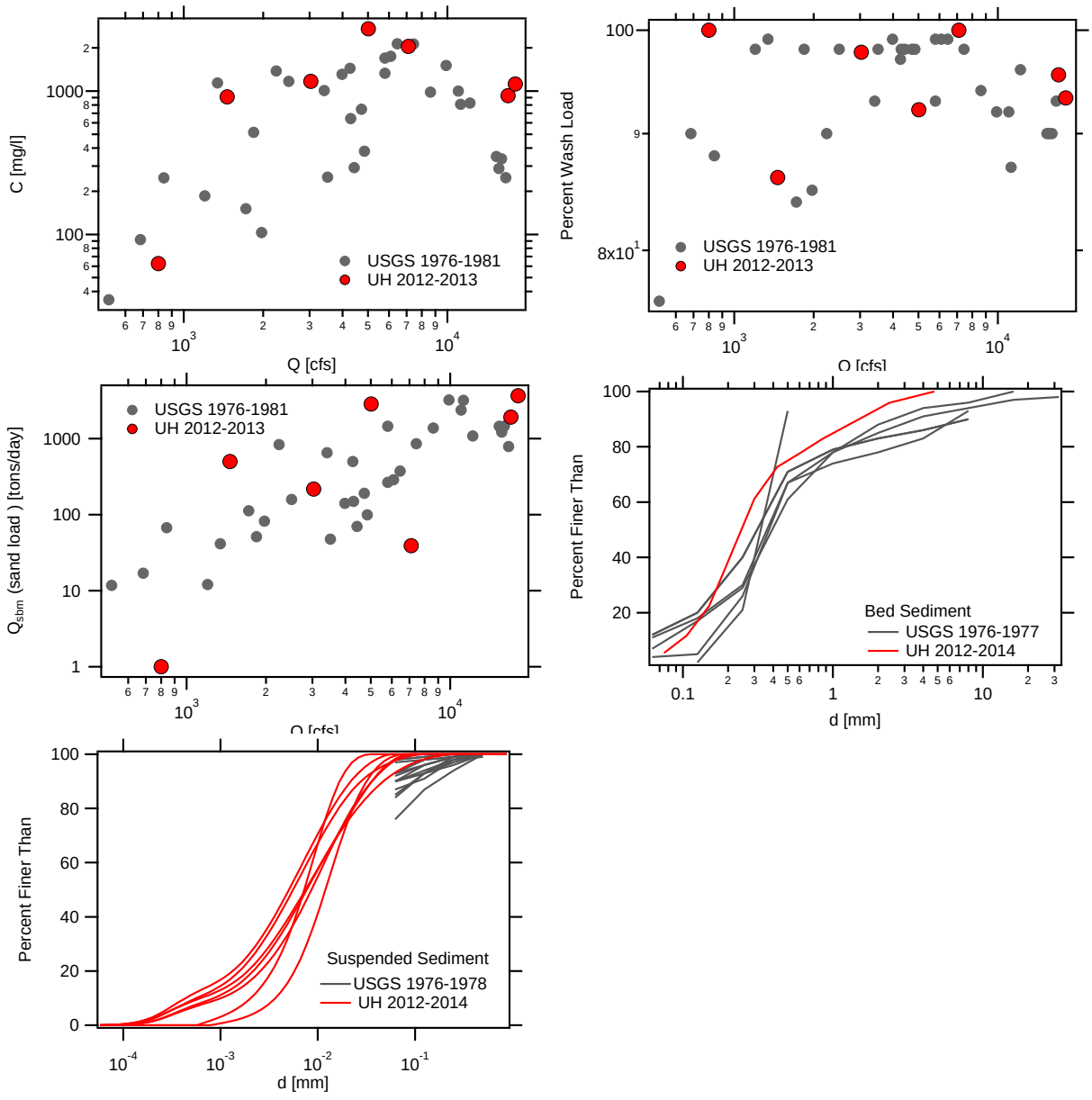

Figure 4.8: Comparison of UH and USGS data at the Oakwood station.

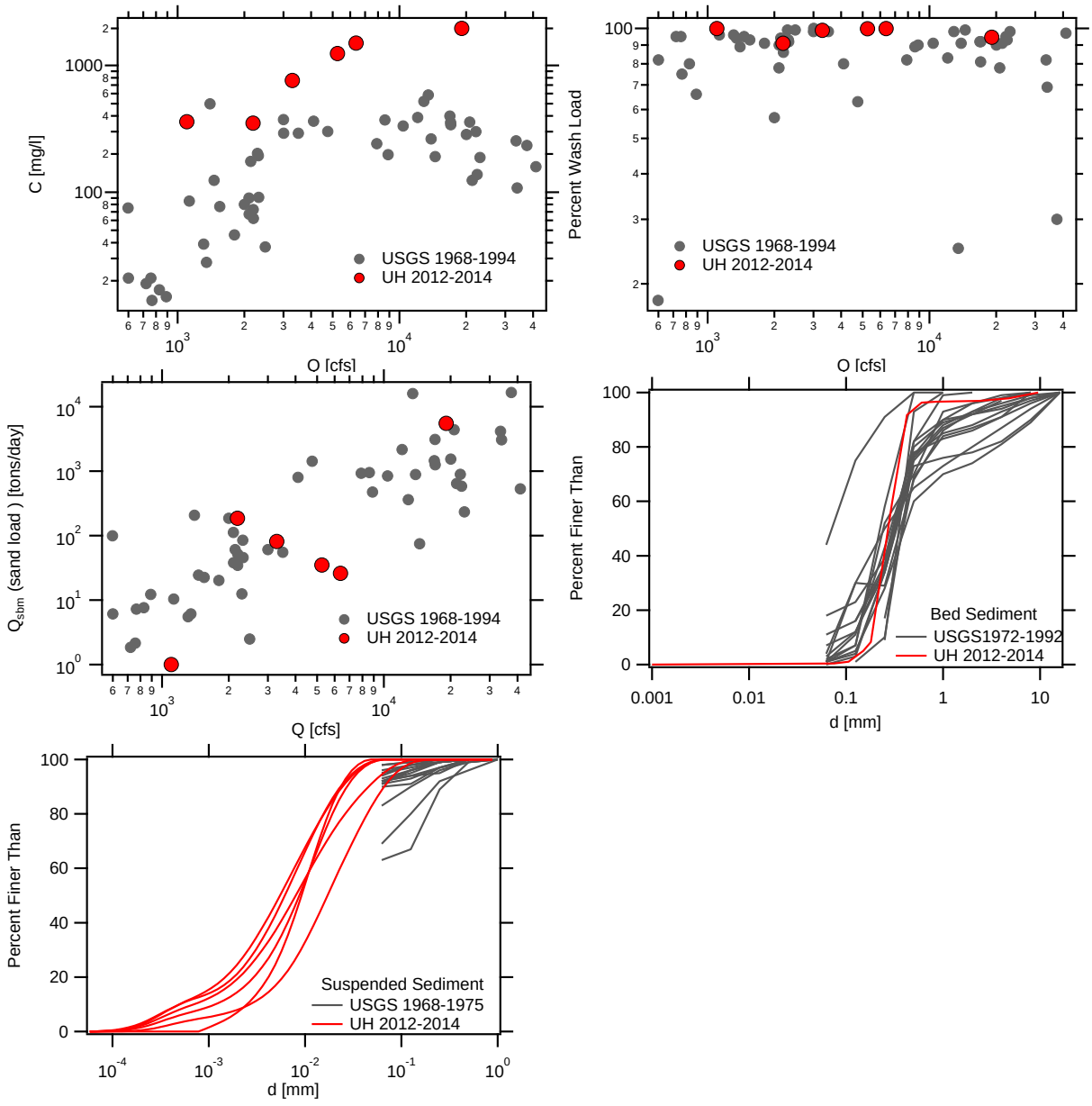

Figure 4.9: Comparison of UH and USGS data at the Crockett station.

5 Analysis and Results

5.1 Sediment rating curves and transport calculations

Sediment rating curves for the suspended load, Q_{sbm}, and the bed load, Q_b, were developed and used to construct the sediment load histograms for the suspended load and bed load independently. The resulting histograms where then added together to produce the total bed material histograms from which the effective discharge was obtained. The suspended sediment rating curves for Q_{sbm} and Q_{ss} were developed using regression and the measured data (figure 5.1). The bed load rating curves were developed by calculating the total bed load in tons per day associated with the daily discharge data at the time of sampling at each site. The paired data was then fit with a power law curve to produce the rating curve. All rating curves retained the power-law functionality of equation 2.3. A list of all coefficients and the correlation coefficient for curve are listed in Table 5.1.

The Einstein-Brown equation was used to calculate bed load. The Einstein-Brown equation uses the original dimensionless parameters defined by Einstein (1942) with the two-part power-law curves of Brown (1950):

$$q_b^* = \begin{cases} 40F(\tau^*)^3 & \text{for } \tau^* \geq 0.182 \\ 2.15Fe^{-0.391/\tau^*} & \text{for } \tau^* < 0.182 \end{cases} \tag{5.1}$$

Here, q_b^* and τ^* are the dimensionless bed load transport rate and dimensionless bed shear stress respectively:

$$q_b^* = \frac{q_{bv}}{\sqrt{R_s g d_{50}^3}}, \quad \tau^* = \frac{\tau_B}{R_s \gamma d_{50}} \tag{5.2}$$

In these definitions, q_{bv} is volumetric bed load transport rate per unit width, τ_B is the bed shear stress, $R_s = (\rho_s - \rho)/\rho$ is the submerged specific gravity, and d_{50} is the sediment size for which 50% of the material is finer than by weight. F in equation 5.1 is the Rubey (1933) settling velocity factor:

$$F = \left[\frac{2}{3} + \frac{36\nu^2}{g d^3 R_s}\right]^{1/2} - \left[\frac{36\nu^2}{g d^3 R_s}\right]^{1/2} \tag{5.3}$$

In the Einstein-Brown equation, the stress driving transport is the stress associated with only the skin friction component of stress. Hence, $\tau_B = \tau'_B$ with,

$$\tau'_B = \gamma R' S = \rho u_*'^2 \tag{5.4}$$

where u'_* is the friction velocity associated with the skin friction and R' is the hydraulic radius associated with skin friction. In this framework, the total hydraulic radius is a summation of the skin and form roughness associated hydraulic radii, $R = R' + R''$ were R'' is due to form roughness. The transport equation is solved using the Einstein skin friction resistance relation:

$$\frac{U}{u'_*} = 5.74 \log\left(12.27 \frac{R'}{d_{65}}\right) \tag{5.5}$$

The depth and geometric properties of the cross section were measured at each site at the time of sampling. Therefore, if S is known, and uniform flow is assumed (i.e., eq. 5.4 is valid), then R' and τ'_B can be calculated using equations 5.4 and 5.5 with U defined from continuity. This procedure for calculating τ'_B was used, and the skin friction component of the bed shear stress was used in the bed load transport calculations with equation 5.1. However, following through with the entire effective discharge analysis using the skin friction shear stress values resulted in very steep bed load rating curves. In turn, the steep rating curves pushed the effective discharge estimates to the very largest flows observed during the period of record. The reason for this is that the shear stress partitioning method produced a difference between the total and skin shear stress that increased with a reduction in mean channel velocity. This amplified the difference in transport capacity between low and high flows. To avoid having the effective discharge land in the largest flow bin, we used the bed shear stress obtained from the total hydraulic radius in all bed load calculations.

Slope measurements were not made at the time of sampling because the surveying equipment available to us (construction level and tape) was not accurate enough to measure the very small slopes on the Trinity. For this reason, values of S were obtained from a USGS database of computed slopes for Texas gaging stations and some additional analysis.

The USGS computed slope used is referred to as the "main-channel slope" (Asquith and Slade, 1997). The main-channel slope is defined as the change in elevation between the two end points of the main-channel divided by the distance, L (Asquith and Slade, 1997). In the calculation method, L is the longest defined channel shown in a 10-meter digital elevation model (DEM) from the approximate watershed headwaters to the point of interest, and the elevation change between the two points is extracted directly from the 10-meter DEM. The main-channel slope is therefore more of a watershed slope based on the channel network than it is a local reach slope. Because of its calculation method, we suspect that the main channel slope values will be, on average, slightly higher than the local reach slopes at the stations because the main channel slope by definition incorporate elevation change further up in the watershed where slopes are likely higher. Nevertheless, this definition of slope was very reasonable for all but the Crockett station. For example, the reported main channel slope at each of the four sites was, Rosser $S = 0.00036$, Trinidad $S = 0.00026$, Oakwood $S = 0.00015$, and Crockett $S = 0.000823$. These main channel slopes would mean that the Crockett site had a slope that was over 5 times greater than the nearest upstream station (Oakwood). Since sediment continually fined in the downstream direction and discharge increased, it did not seem reasonable to use the 0.000823 value for the slope at Crockett. Instead, slope was estimated using the measured cross sectional geometry during the time of sampling and the USGS 15-min discharge data. Using this data, a slope was calculated for each flow condition using the Manning equation and assumed n values ranging from 0.03 to 0.04. The average of all back calculated slopes was then taken and used for the slope at Crockett. This analysis yield a slope of $S = 0.00012$, which seemed to be reasonable given that the upstream slope at Oakwood was $S = 0.00015$.

Slope estimates for Crockett were also obtained using the local floodplain elevation and the river length over 10's of kilometers. Doing so produced slopes with an average of 0.0002; a value slightly steeper than the slope used for Oakwood, but much less than the 0.000823 value in the USGS database. Phillips (2008) also tried several methods for estimating slope and water surface slope at Rosser, Trinidad, Oakwood, and Crockett. Similar to our analysis, Phillips reported that the calculated values and trend in slope progressing downstream varied depending

on the method used to calculate slope. Sometimes slopes continually decreased. Other times they fluctuated between increasing and decreasing. For his stream power estimation, Phillips use a decreasing slope going from Oakwood to Crockett as we have done here. The full analysis described below was done using several different slope values for Crockett; some of which were steeper than Oakwood and some that were lower. In the end, the exact slope value did not impact the effective discharge calculation. The exact slope value did, however, play a very large role in the calculated annual sediment yield (discussed in more detail in section 5.3).

A summary of all measured and calculated sediment loads used in development of the rating curves is given in Table 5.2. The table also lists the total calculated sediment loads of

$$Q_{tl} = Q_{sbm} + Q_b \tag{5.6}$$

which includes the bed load and the suspended load;

$$Q_{\text{sed-all}} = Q_{ss} + Q_b \tag{5.7}$$

which includes bed load, suspended load, and wash load; and the SAMwin derived total bed material load Q_{tl}. The SAMwin derived Q_{tl} was developed using the measured cross sectional data and the computer program SAMwin, a Windows version of the SAM Hydraulic Design Package For Channels. The Einstein total load equation was used for calculating the total loads with SAMwin.

For most cases, the calculated bed load was greater than the measured suspended bed material load. This can be seen from the rating curves (figure 5.1) and the tabulated values in Table 5.2. Part of this might be somewhat artificial due to the use of τ_B rather than τ'_B in the bed load calculations. However, a large component is certainly a result of very little sand being physical captured in either the bucket or the depth-integrated sampler during the majority of the sampling trips. Two potential reasons for the low sand content could be, (1) that the sampler wasn't physically capturing sand that was suspended high up in the water column, or (2) very little sand actually made up into the water column past the first few inches from the bed.

To further investigate the lack of sand in the samples, we examine the predicted sand concentration profile to see how the bed material d_{50} should theoretically have been distributed in the water column. To do this, we examined the Rouse number,

$$Z^* = \frac{w_s}{\kappa u'_*} \tag{5.8}$$

and the vertical sand flux profile for each sample location and day. In equation 5.8, w_s is the settling velocity of the bed material d_{50} and κ is the von Karman constant ($\kappa = 0.4$). The standard equilibrium Rouse profile with a Schmidt number of 1 without buoyant damping was used to develop $C = C(z)$ at each condition. This was then multiplied with the velocity profile of Wright and Parker (2004) to obtain the suspended sand flux profile. For the Rouse profile calculations, a reference height of $0.05h$ was used along with the reference concentration prediction and shear stress partitioning methods of Wright and Parker (2004). The sand flux profile was then used to locate the height at which 90% of the total suspended sand flow rate is reached, h_{ss90}. If the total unit width sand flow rate is:

$$q_{ss} = \int_{z=0}^{z=h} uCdz, \tag{5.9}$$

then h_{ss90} is the depth that satisfies the following:

$$0.9q_{ss} = \int_{z=0}^{z=h_{ss90}} uCdz. \tag{5.10}$$

The theoretical calculations showed that the Rouse number ranged from 1 to 5, and that h_{ss90} most often occurred within the first meter from the bed (Table 5.2). In fact, in several cases, 90% of the suspended sand load was predicted to occur within the first 10 cm from the bed. Sampling suspended sand traveling this low is problematic. This is true for the bucket sampler since it collects water and sediment near the free surface. And, it is also an issue for the depth integrated sampler since the US DH-2 cannot sample the first 4 in (10 cm) from the bed due to its physical construction and nozzle location. Unfortunately, no clear h_{ss90} threshold was found from the analysis to predict when the depth-integrated sampler would or would not capture sand. Nevertheless, in a broad generalization, the analysis suggests that the Trinity is bed load dominated and that the majority of suspended sands likely travel very close to the bed.

	Q_{sbm} [tons/day]			Q_{ss} [tons/day]			Q_b [tons/day]			Q_{SAM} [tons/day]		
Site	α	β	R^2	α	β	R^2	α	β	R^2	α	β	R^2
Rosser	0.005	1.220	0.24	0.229	1.249	0.94	0.011	1.362	0.97	3.0E-05	2.065	0.92
Rosser (USGS)*	1E-05	1.992	0.69	0.200	1.209	0.72						
Trinidad	6E-06	1.944	0.57	0.161	1.325	0.99	0.002	1.733	0.97	9.9E-02	1.173	0.90
Trinidad (USGS)*	6E-05	1.715	0.64	0.003	1.594	0.80						
Oakwood	1E-04	1.761	0.50	0.010	1.640	0.79	0.048	1.399	0.99	4.0E-06	2.371	0.97
Oakwood(USGS)*	8E-04	1.520	0.63	0.018	1.538	0.72						
Crockett	3E-07	2.288	0.64	0.006	1.697	0.97	1.360	0.903	0.93	3.0E-07	2.527	0.95
Crockett (USGS)*	1E-04	1.624	0.66	0.004	1.553	0.81						

Table 5.1: Rating curve coefficient values and correlation coefficients. *Rating curves developed using all of the historic USGS data at the site along with the additional data collected by UH. Rating curves have the form of $Q_i = \alpha Q^{\beta}$ where i is the transport mode.

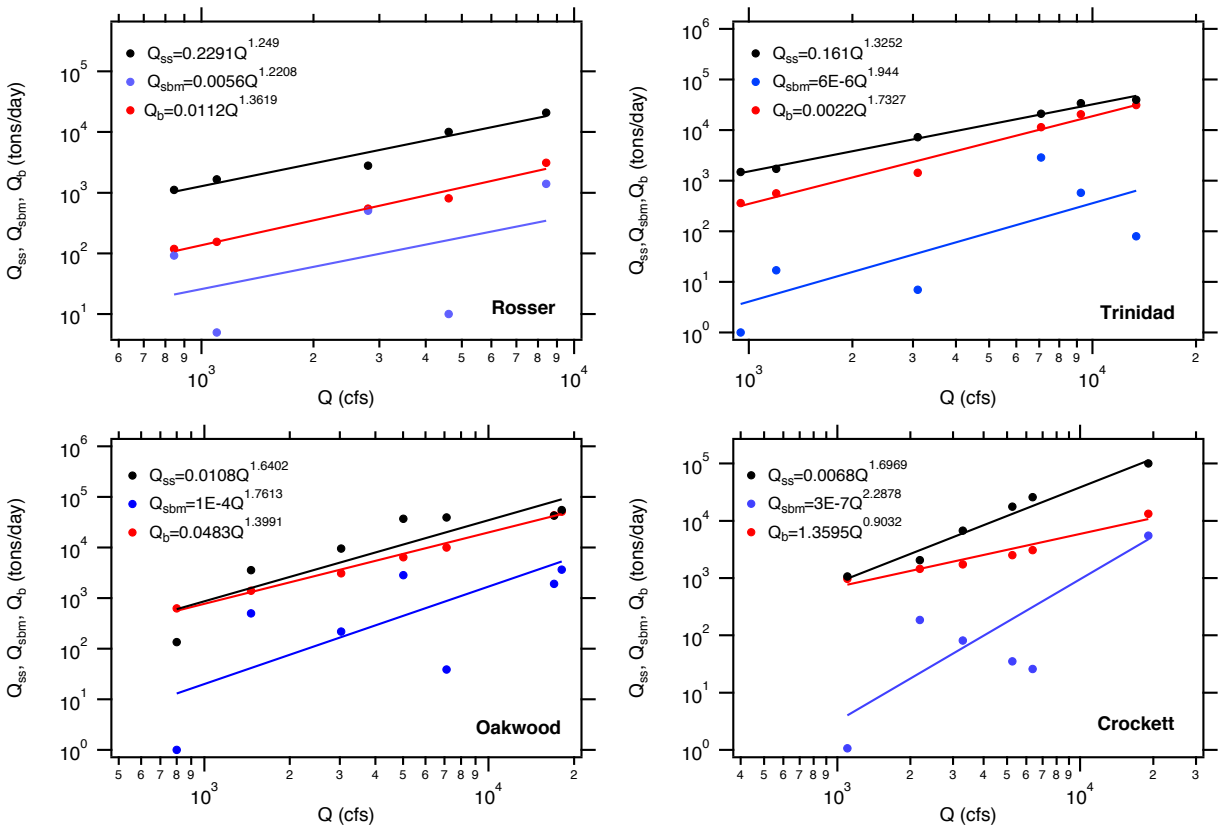

Figure 5.1: Rating curves.

Site	Date	Condition	S	Q [cfs]	d_{50} [mm]	d_m [mm]	τ^*/τ^*_{cr}	z_*	h^1_{ss90} [m]	Q_{ss} [T/day]	Wash Load [%]	Q_{sbm} [T/day]	Q_b [T/day]	$Q_{\text{sed-all}}$ [T/day]	Q_{tl} [T/day]	SAM Q_{tl} [T/day]
Rosser	5/17/12	Low	0.000357	844	3.13	5.8	2	11.4	0.05	1115	92	93	119	1234	211	33
Rosser	6/9/12	Moderate	0.000357	2800	3.13	5.8	3	7.9	0.10	2794	82	506	544	3338	1050	394
Rosser	10/27/12	Low	0.000357	1100	3.13	5.8	2	10.1	0.05	1661	100	5	155	1816	160	57
Rosser	4/5/13	Moderate	0.000357	4610	3.13	5.8	3	5.4	0.11	10072	100	10	811	10882	821	1103
Rosser	5/17/13	High	0.000357	8410	3.13	5.8	5	5.9	0.17	20869	93	1398	3129	23998	4527	3818
Trinidad	5/17/12	Low	0.00026	946	0.65	0.93	7	4.8	0.06	1480	100	1	361	1841	363	306
Trinidad	6/9/12	Moderate	0.00026	7080	0.65	0.93	17	3.5	0.22	21006	86	2878	11475	32480	14352	3249
Trinidad	10/27/12	Low	0.00026	1200	0.65	0.93	8	4.6	0.07	1715	99	17	560	2275	577	405
Trinidad	1/12/13	High	0.00026	13400	0.65	0.93	22	3.5	0.30	39757	100	80	31111	70868	31190	6866
Trinidad	3/13/13	Moderate	0.00026	3100	0.65	0.93	9	3.0	0.13	7274	100	7	1433	8707	1440	1233
Trinidad	5/18/13	High	0.00026	9240	0.65	0.93	20	3.6	0.27	33894	98	576	20506	54400	21083	4440
Oakwood	5/17/12	Low	0.000147	1460	0.25	0.57	17	2.7	0.21	3584	86	498	1402	4985	1900	127
Oakwood	10/27/12	Low	0.000147	800	0.25	0.57	13	3.7	0.13	135	100	1	626	761	627	31
Oakwood	5/18/13	Moderate	0.000147	5010	0.25	0.57	27	1.4	1.02	36755	92	2850	6433	43188	9283	2368
Oakwood	5/24/13	Moderate	0.000147	3030	0.25	0.57	22	1.8	0.60	9562	98	217	3070	12632	3288	719
Oakwood	10/31/13	High	0.000147	18100	0.25	0.57	41	1.5	1.58	54629	93	3660	51077	105705	54737	49776
Oakwood	11/1/13	High	0.000147	17000	0.25	0.57	39	1.5	1.50	42643	96	1919	43431	86074	45350	42900
Oakwood	6/27/14	Moderate	0.000147	7110	0.25	0.57	30	1.3	1.31	39313	100	39	10000	49313	10039	5431
Crockett	5/17/12	Low	0.00012	2190	0.28	0.47	12	3.3	0.16	2067	91	186	1452	3519	1638	83
Crockett	10/27/12	Low	0.00012	1100	0.28	0.47	11	4.0	0.10	1068	100	1	973	2041	974	15
Crockett	5/25/13	Moderate	0.00012	3290	0.28	0.47	13	3.3	0.17	6744	99	81	1737	8481	1818	232
Crockett	6/13/13	Moderate	0.00012	5260	0.28	0.47	15	2.3	0.35	17592	100	35	2509	20102	2545	759
Crockett	11/1/13	High	0.00012	19100	0.28	0.47	18	1.5	1.37	100972	95	5523	13331	114303	18854	19738
Crockett	6/27/14	Moderate	0.00012	6370	0.28	0.47	15	2.0	0.48	25772	100	26	3087	28858	3112	1231

Table 5.2: Summary of sediment transport calculations. [1] h_{ss90} is the predicted distance above the bed for which 90% of the total suspended sand load passes beneath; the calculate is based on d_{50} of the bed material. *Wash load values used in the development of the sediment rating curves.

5.2 Effective discharge calculations

5.2.1 Development of the daily flow PDF

The developed rating curves were used in conjunction with the flow duration histograms (pdf of the daily flow discharge) to build the sediment transport histograms as a function of daily flow levels (fig. 2.2). The flow duration histograms, S_h (equation 2.2), were computed two different ways. In the first, the histogram was developed by manually selecting the discharge bin width and sorting the observed daily flow data. In the second, the histogram was generated objectively using the kernel density method of Klonsky and Vogel (2011).

For the manual method, the discharge bin widths were first set to an evenly spaced 25 bins over the range of observed data at each site following the recommendations of Hey (1997), and Biedenharn et al. (2000). However, when doing this, it was most often the case that the first bin in the sediment histogram, S_h, contained the greatest percentage of sediment; this would result in the effective discharge being defined as the discharge equal to the midpoint discharge of the first bin. When this occurred, the number of bins was increased in increments up to a total of 40 or 50 bins in an attempt to produce a smoother histogram.

During this process of manually modifying the discharge bin widths, it was observed that the selection of the bin width greatly impacted the final effective discharge estimates. In an effort to avoid the subjectiveness of the bin width selection, a second, more objective, method for creating the flow duration histogram was used. The method used was the kernel density estimation method of Klonsky and Vogel (2011). The details of the kernel density method are discussed in Klonsky and Vogel (2011) and in Strom and Rouhnia (2013).

5.2.2 Sediment transport effectiveness distributions

Effective discharge estimates, Q_e, were made directly from sediment transport effectiveness histograms, S_h (Wolman and Miller, 1960), that were developed using both the manual and kernel density pdfs of the flow. The S_h distributions were developed by multiplying the load at a particular discharge as estimated by the rating curves with the pdf of the daily flow discharge (equation 2.2). This was done independently for the bed load, Q_b, and suspended bed material load, Q_{sbm} as follows:

$$S_{h:sbm} = Q_{sbm} f_Q \tag{5.11}$$

$$S_{h:b} = Q_b f_Q \tag{5.12}$$

with the total transport effectiveness distribution being the summation of the bed and suspended load,

$$S_h = S_{h:sbm} + S_{h:b} \tag{5.13}$$

For the manually developed histograms, the discharge at the midpoint of the discharge bin was used to calculate that daily loads from the rating equations. For the kernel density method, the Q values used corresponded with 100 regularly spaced values for which f_Q was calculated. The sediment effectiveness distributions were calculated using the rating curves developed using (1) only data from this study, (2) using all available USGS data plus the data from this study, and (3) using the SAMwin rating curves. Coefficients for all of these rating curves can be found in

Table 5.1. Figures 5.2 and 5.3 show these effectiveness distributions developed using the data obtained in this study.

All of the S_h distributions show the dominance of bed load transport over suspended load for the study sites (figures 5.2 and 5.3). This is to be expected from the Rouse numbers and h_{ss90} values (table 5.2) and the developed rating curves (figure 5.1). Because of the dominance of bed load, which was a calculated in our analysis, we also ran the effective discharge calculations using other bed load transport equations. The other equations tested included: the Meyer-Peter and Müller (1948) equation and the standard Einstein bed load formula. Using other bed load formulas did change the magnitude of the calculated bed load, but it did not simnifically change the shape of the sediment transport effectiveness histograms. Therefore, the use of different equations did not significantly alter the final effective discharge. Nonetheless, the dominance of bed load in the calculations and lack of physical bed load samples should be considered as a limitation of this study.

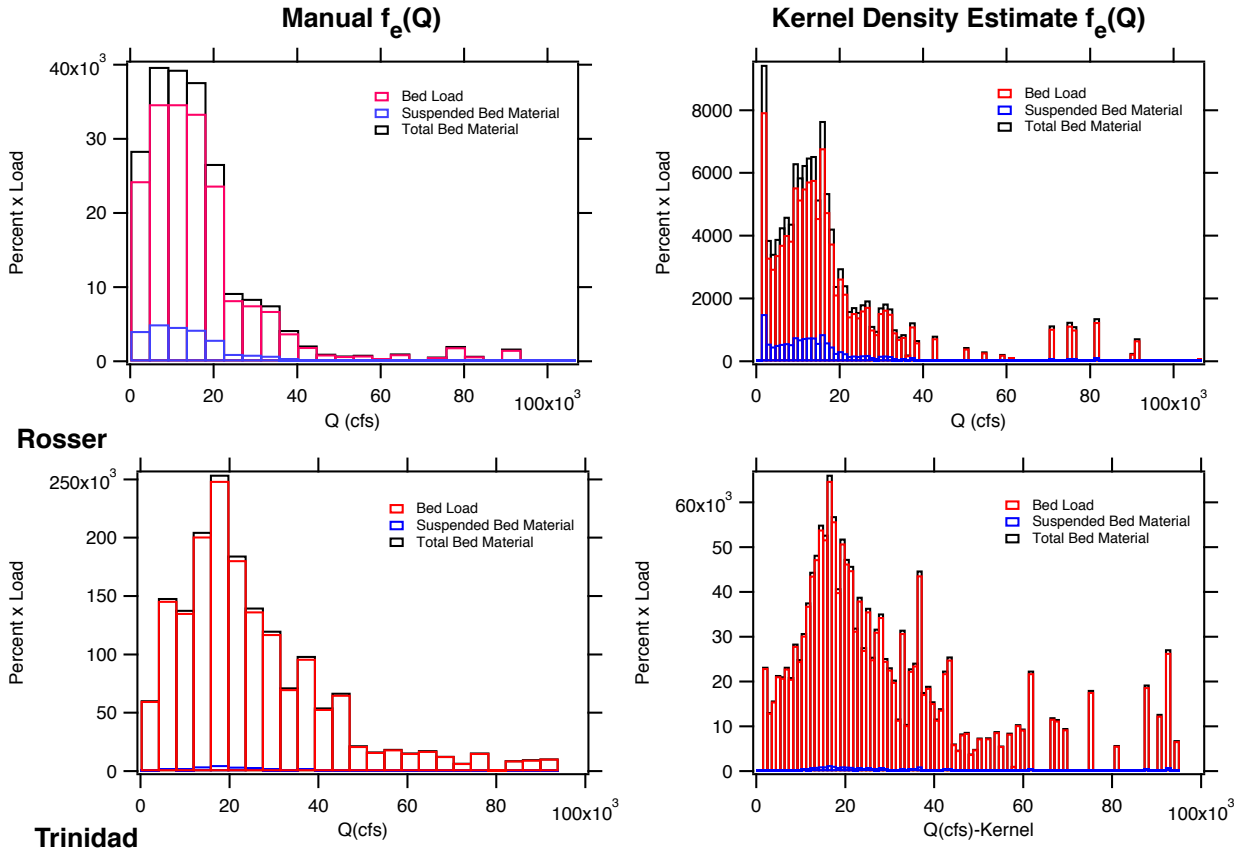

Figure 5.2: Sediment transport effectiveness distributions for Rosser and Trinidad using both the manual and kernel density estimate derived daily flow pdfs.

5.2.3 A note on picking the effective discharge

The effective discharge is defined as being the discharge associated with the peak or highest value of S_h. However, for some station, S_h does not monotonically increase smoothly from zero

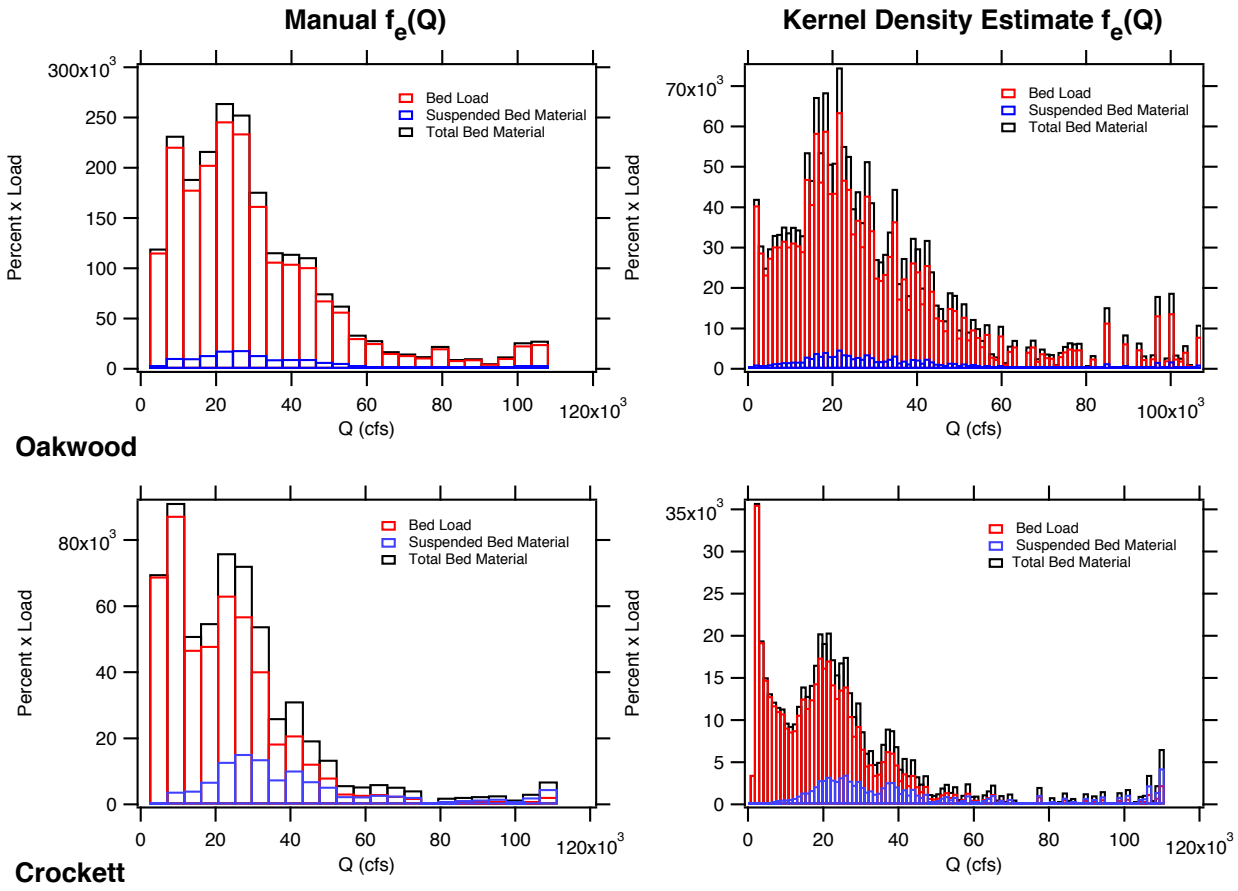

Figure 5.3: Sediment transport effectiveness distributions for Oakwood and Crockett using both the manual and kernel density estimate derived daily flow pdfs.

up to the peak value and then monotonically fall back down to zero with increasing discharge as conceptualized in figure 2.2 and in Wolman and Miller (1960). Sometimes, the maximum value of S_h is a lone, isolated bin (figure 5.2 for Rosser using the kernel density methods and 5.3 for Crockett). Often times, this lone peak occurs in one of the first few bins, and selection of such a discrete peak would lead to effective discharges associated with the lowest flows in the river. Additionally, the problem of an isolated peak can come and go depending on the exact number of bins and bin widths used; making the selection of effective discharge vary dependent on the method used for generating the discharge pdf.

To avoid the lone-peak problem, we have followed the suggestion of Biedenharn et al. (2000) by fitting a smooth and continuous line through the entire S_h distribution by eye. The effective discharge is then chosen as the peak of this smooth distribution. While this method does retain a measure of user subjectiveness, the method does produces more consistent results for the effective discharge, and it keeps high frequency but very low magnitude flows (or low frequency but high magnitude flows) from being assigned as the effective discharge.

5.2.4 The effective discharge values

The effective discharge was selected using the smoothing method described above from each of the sediment effectiveness histograms generated using (1) only data from this study, (2) using all available USGS data plus the data from this study, and (3) using the SAMwin rating curves. For each, the effectiveness histograms were generated with both the manual and kernel density method for generating the flow pdf. The values of effective discharge obtained from these three sets of rating curves and the two different flow pdf generation methods are given in Table 5.3. Very little difference was found in the computed effective discharge when using the rating curves developed with only the UH measured data for the suspended bed material compared to those developed using the UH plus USGS data (Table 5.3). The only small difference between the USGS+UH and UH only was for the effective discharge estimate at Rosser where the rating curve with the UH only data produced an effective discharge of 11,102 cfs compared to the 15,543 cfs (one bin to the right) produced with the added USGS data. In the remainder of the report, only the rating curves developed with the measured data from this study are used.

	Q_e using Manual $f_e(Q)$		Q_e using Kernel $f_e(Q)$		Different Q_e values by method?		
Station	Measured [cfs]	SAM [cfs]	Measured [cfs]	SAM [cfs]	Manual vs Kernel $f_e(Q)$	Measured vs SAM	UH vs USGS+UH[3]
Rosser	11,102	15,543	15,099	15,099	yes	yes (no)[1]	yes[2]
Trinidad	17,535	17,535	15,742	15,742	no	yes (no)	no
Oakwood	19,781	24,177	20,820	20,820	no	yes (no)	no
Crockett	20,345	24,866	20,593	21,169	no	yes (no)	no

Table 5.3: Comparison of calculated effective discharge using both the manual and kernel density estimation for $f_e(Q)$ along with the effective discharge values obtained using the total load rating curves via SAM. The right three columns give an indication of how dependent the calculated Q_e value is on, (1) the method used to develop $f_e(Q)$, (2) whether or not measured suspended load plus calculated load is used instead of a single calculated total load, and (3) whether or not all of the historic USGS data is used in addition to the data measured in this study for suspended bed material.
[1]The first response is for the difference between the measured and SAM using the manual $f_e(Q)$; values in parenthesis are for the kernel density estimate of $f_e(Q)$.
[2]Comparisons made for the manually developed $f_e(Q)$ only. For Rosser, the USGS+UH rating curve yields $Q_e = 15,543$ cfs.

In addition to the effective discharge, we also calculated the half-load sediment discharge, $Q_{1/2}$ from cumulative distributions of the sediment moved as a function of discharge. These values and the cumulative curves for the amount of water and sediment moved during the analysis time period as a function of discharge are shown in figures 5.4 and 5.5. The plots shown in these figures are similar to the suggested summary plots of Klonsky and Vogel (2011) (i.e., figure 10 in their paper). The plots can be used to easily see what the fraction of water moved by flows less than (or greater than) a particular discharge is and what percentage of sediment moved this corresponds to. For example, at Trinidad (figure 5.4), the figure can be used to see that about 50% of the water volume is moved by discharges less than approximately 10,000 cfs, but that discharges less than 10,000 cfs only transport about 25% of the sediment passing the station. The plots can also be used to show what the total fraction of sediment moved by flows equal to

and less than the effective discharge. For example, at Trinidad, flows equal to and less than the effective discharge are responsible for transporting just under 50 % of the total sediment load.

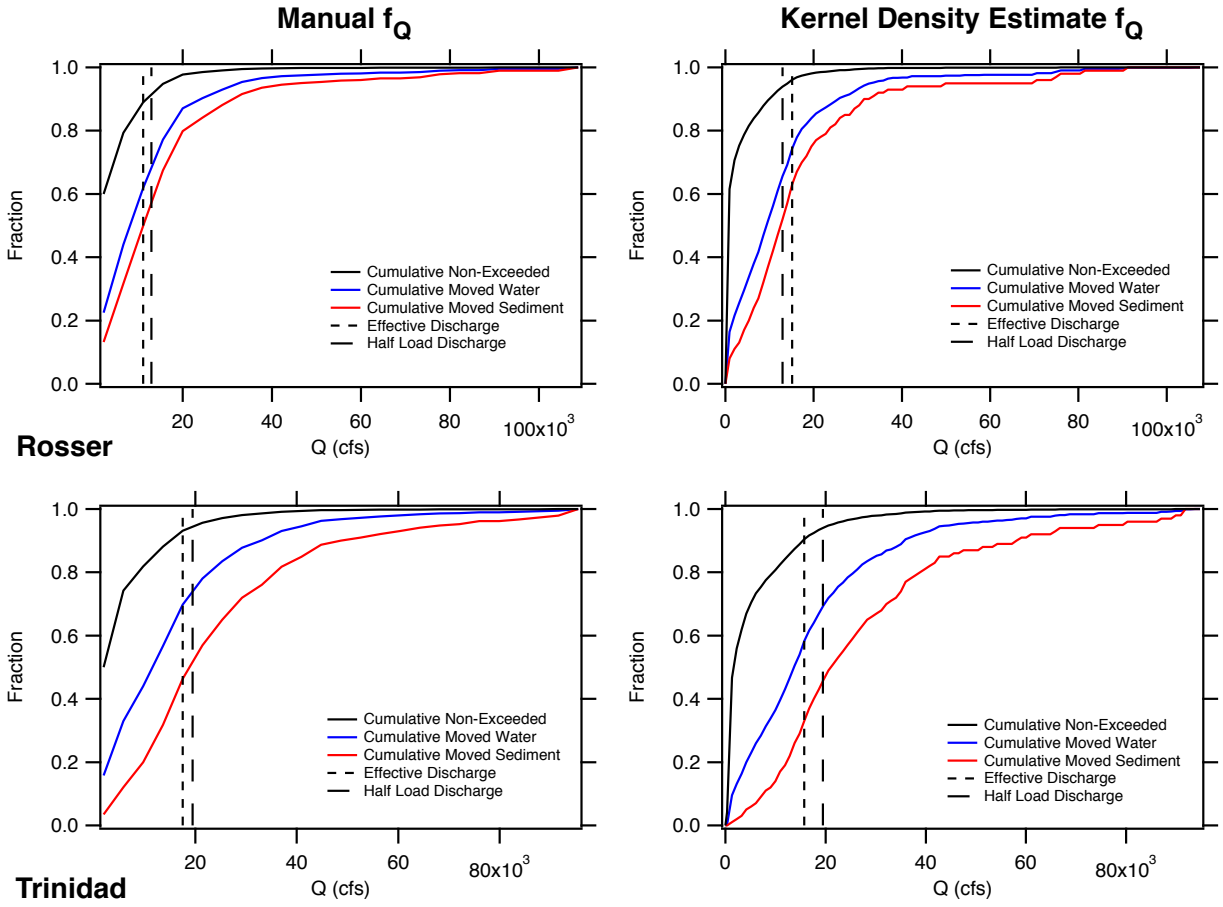

Figure 5.4: Summary plots showing the cumulative fraction of flow and sediment moved as a function of discharge, the flow non-exceedance curve, the sediment effective and half-load discharges for Rosser and Trinidad using the manual and kernel density estimate derived daily flow pdfs.

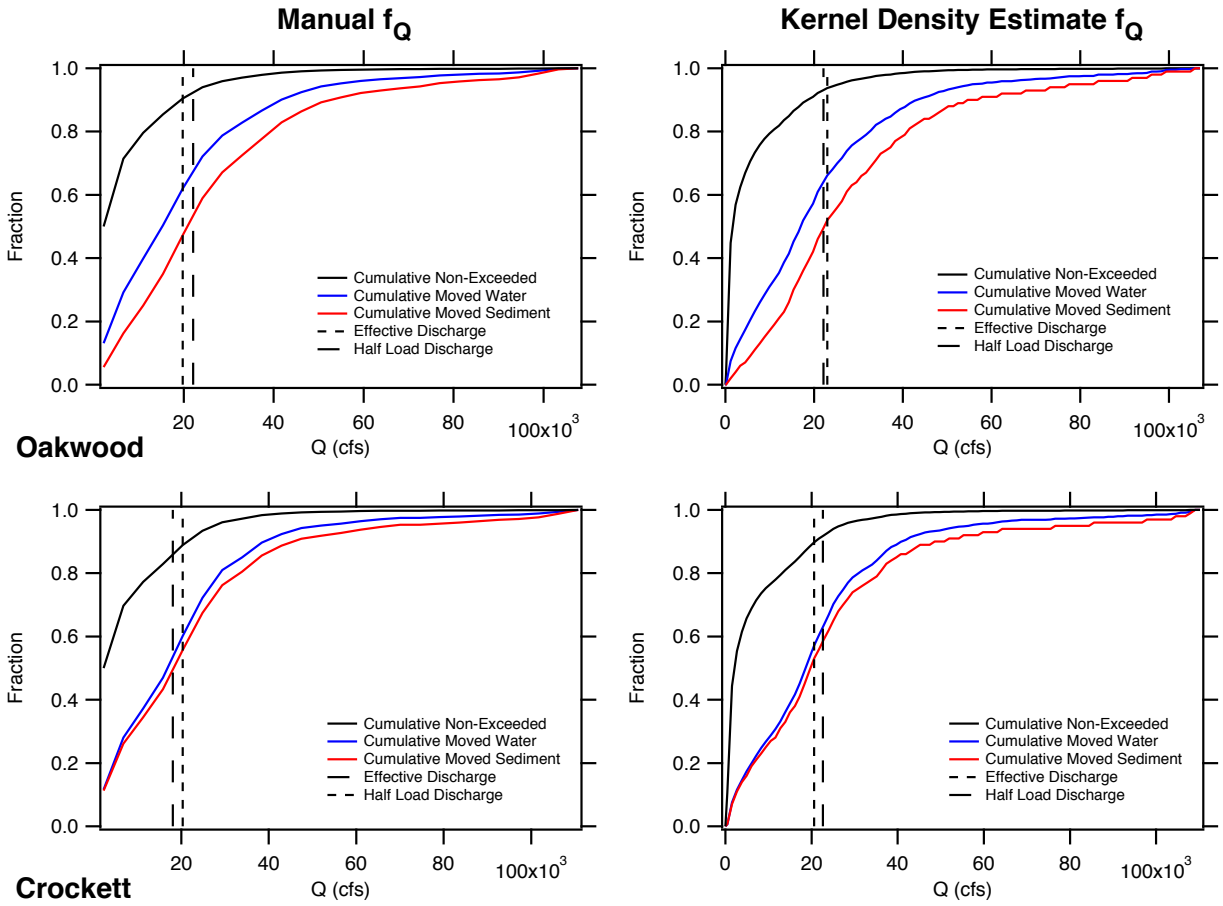

Figure 5.5: Summary plots showing the cumulative fraction of flow and sediment moved as a function of discharge, the flow non-exceedance curve, the sediment effective and half-load discharges for Oakwood and Crocket using the manual and kernel density estimate derived daily flow pdfs.

A comparison of the effective discharge and half-load discharge data along with the fraction of time that flows exceeded the effective discharge, the fraction of sediment carried by flows less than the effective discharge, and the calculated return period of the effective discharge for both the manual and kernel density estimation methods are given in table 5.4. Effective discharge calculated using the two different methods for developing f_Q were fairly equivalent; especially when using the smoothed distribution method. Because the kernel density method can be quite sensitive to loan peaks, we suggest that the load histograms obtained with the manual developed daily flow pdfs are the best for estimating the effective discharge and half-load discharge for the four gage stations.

	Manual $f_e(Q)$					Kernel Density Estimate of $f_e(Q)$				
Station	Q_e [cfs]	$Q_{1/2}$ [cfs]	PT Q_e exceeded	PS carried by $Q < Q_e$	T_R [yr]	Q_e [cfs]	$Q_{1/2}$ [cfs]	PT Q_e exceeded	PS carried by $Q < Q_e$	T_R [yr]
Rosser	11,102	11,963	11	32	1.0	15,099	12,924	4	57	1.0
Trinidad	17,535	19,483	7	32	1.0	15,742	20,559	10	29	1.0
Oakwood	19,781	22,089	10	35	1.2	20,820	23,002	8	42	1.2
Crockett	20,345	18,084	11	43	1.1	20,593	20,033	10	49	1.2

Table 5.4: Effective discharge summary table. PT: percentage of time that the effective discharge, Q_e is exceeded. PS: percentage of sediment carried by flows less than the effective discharge. T_R: return period of the effective discharge.

5.2.5 Relation between effective discharge, half-load discharge, and bankfull discharge

A reasonable question to ask is how the calculated effective discharges computed with the total load sediment histogram (equation 5.13) compare with (1) the effective discharge calculated using only the suspended bed material load histogram (equation 5.11), (2) the sediment half-load discharge calculated using total load, (3) the bankfull discharge, and (4) the 1.5 year return period flows at each of the sites. Calculation of the half-load discharges was done using the cumulative sediment loading curve as a function of discharge as described above.

A description of how each of these values was calculated has been given above for all discharges other than the bankfull discharge. The bankfull discharge, Q_{bf} is defined as the discharge that just fills the main channel up to the top of its banks with water. There are two primary methods for calculating the bankfull state. In the first, the bankfull cross section can be defined in the field using the geometric properties of the cross section and vegetation indicators. The discharge can then be calculated knowing the bankfull geometry, the channel slope, and the roughness coefficient (such as the Manning n value). It can also be defined using a measured range of discharges and geometric properties, e.g., stage or top width as a function of discharge. In this study, we have calculated the bankfull discharge using USGS stage discharge data at each site. With this second method, the bankfull state is defined as the discharge after which there is a change in the stage discharge functionality. The slope break can be viewed as the discharge at which water begins to spill out of the main channel and onto the wider flood plain.

The estimated bankfull discharges are listed in Table 5.5 along with the other dominant discharge estimators. The bankfull discharge increases slightly in the downstream direction. However, this increase is more of a step change in discharge between Trinidad and Oakwood rather than a continuous change. Bankfull and 1.5 return period discharge are close in magnitude for all location.

In general, both the effective and half-load discharges are less than both the bankfull and 1.5 year flows. The effective discharge calculated using the total load histogram did not always aligned with those produced using the suspended bed material load only. The reason for this is that bed load makes up a very large fraction of the total load in our calculations (figures 5.2 and 5.3).

	Total Load[1]		Suspended[2]	Pure Flow Metrics		
Station	Q_e [cfs]	$Q_{1/2}$ [cfs]	Q_e [cfs]	Q_{bf} [cfs]	$Q_{1.5}$ (20 yrs) [cfs]	$Q_{1.5}$ (All yrs) [cfs]
Rosser	11,102	11,963	6,661	26,000	29,543	20,800
Trinidad	17,535	19,483	17,535	25,000	26,600	25,650
Oakwood	19,781	22,089	27,365	32,000	28,200	22,500
Crockett	20,345	18,084	34,031	33,300	30,100	25,700

Table 5.5: Final effective discharge, Q_e, half-load discharges, $Q_{1/2}$, and bankfull discharges, Q_{bf}, at each of the four stations.
[1]Effective and half-load discharges calculated using the total load histogram, $S_h = S_{h:sbm} + S_{h:b}$.
[2]Effective discharges calculated using the suspended bed material load histogram only, $S_{h:sbm}$.

5.3 Annual sediment yield

The annual sediment yield at each station was calculated using the daily flow data and the rating curves developed for bed load and suspended load. These were integrated over a one-year time period to produce a load associated with each year. Plots of the yearly loads from January 1, 1980 to December 31, 2012 are shown below in figure 5.6. In general, the total yearly bed material load increases moving downstream. The exception to this is the Crockett station. The likely cause of this is the low slope of the bed load rating curve (Table 5.1).

Two items of note with the yield calculations are that, (1) the yield is almost all based on the bed load calculations, and (2) as such, calculated yields are very sensitive to small changes in the channel slope. For example, changing the slope at Crockett from 0.00012 to 0.00018 results in a change in the annual yield from what is shown in figure 5.6 to what is shown in figure 5.7. Setting the slope at Crockett equal to $S = 0.0002$ produces yearly yields that are equal to or slightly greater than those at Oakwood. It is worth noting that the total sediment yield should increase in the downstream direction since water and sediment is being collected from a larger and larger area as one moves downstream.

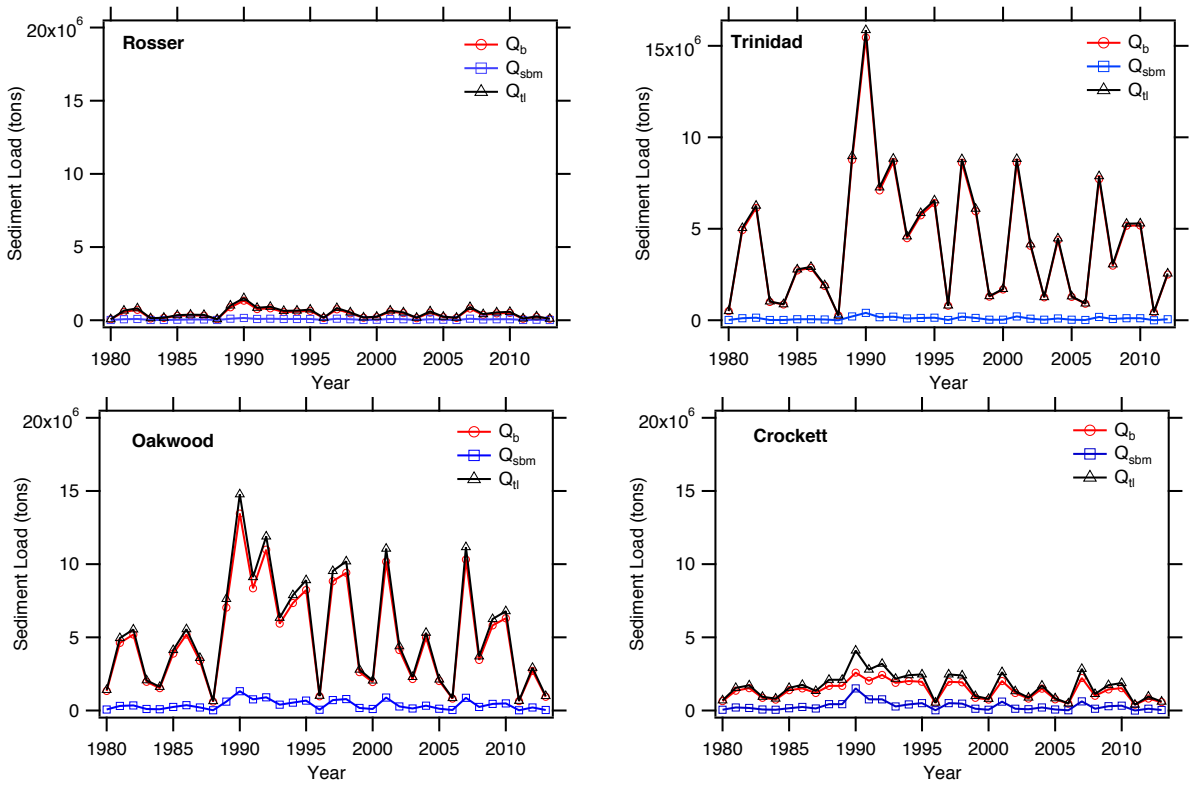

Figure 5.6: Yearly bed material loads at each of the four stations from 1980 through 2013. Q_b is the calculated bed load, Q_{sbm} is the suspended bed material load, Q_{tl} is the total bed material load, $Q_{tl} = Q_b + Q_{sbm}$.

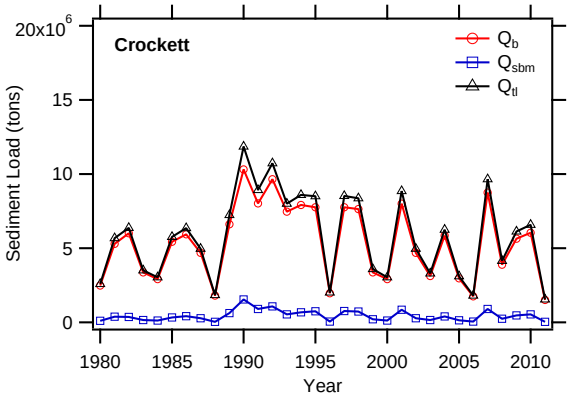

Figure 5.7: Yearly bed material load calculated for Crockett using a slope of $S = 0.00018$.

6 Conclusions

6.1 Summary

The effective discharge was calculated at four stations along the Trinity River using historic USGS daily flow data along with rating curves developed from measured suspended sediment data and calculated bed load transport rates. Measurements for the analysis of channel cross sectional properties, bed sediment, and suspended sediment concentration were made periodically between May 17, 2012 and June 27, 2014. The effective discharge estimates were made using probability density functions of the daily discharge created using histograms with manually set bin width and the kernel density estimation method (Klonsky and Vogel, 2011). Sediment half-load discharges and cross sectional bankfull discharges were also calculated. The rating curves developed in this study were also used to estimate the yearly bed material yield at each station for the time period from January 1, 1980 to December 31, 2012.

6.2 Main findings

A summary of the calculated effective discharge values can be found in table 5.5 along with other measures of dominant discharge such as the half-load discharge, the bankfull discharge, and the 1.5 year return period discharge for each station. Results showed that the calculated effective discharges increased in the downstream direction from 11,102 cfs at Rosser to 20,345 cfs at Crockett.

Other items of note with respect to the effective discharge calculation were that the calculated discharges are, (1) fairly insensitive to whether or not the newly measured suspended sediment data was supplemented with the historic USGS data when developing the rating curves for the suspended sediment; (2) generally independent of the method used to develop the pdf of the daily flow (the exceptions to this occurred at Rosser); and (3) general insensitivity to whether or not measured data was used in developing the rating curves for suspended sediment load (only 1 out of 4 stations produced different Q_e values when using only the Einstein total load equation in SAMwin).

The dominant discharge range for the middle Trinity (i.e., that discharge for which the river is morphologically responding to) based on the calculations in this report is from 15,000 to 20,000 cfs. The average half-load discharge for all four stations would also fall within this range. The bankfull and $Q_{1.5}$ flows at the four stations were found to generally be larger than the effective or half-load discharges and to fall within the range of 25,000 to 30,000 cfs. Estimated return periods for the effective and half-load discharges varied from 1 to 1.2 years.

References

Andrews, E. D. (1980). Effective and bankfull discharges of streams in the Yampa River basin, Colorado and Wyoming. *Journal of Hydrology*, 46(3-4):311–330.

Asquith, W. H. and Slade, R. M. (1997). Regional equations for estimation of peak- streamflow frequency for natural basins in Texas. Technical report, U.S. Geological Survey Water- Resources Investigations Report 96–4307.

ASTM (2007). ASTM d3977 - 97(2007) standard test methods for determining sediment concentration in water samples. *American Society for Testing and Materials*, 11.02.

Biedenharn, D. S., Copeland, R. R., Thorne, C. R., Soar, P. J., Hey, R. D., and Watson, C. C. (2000). Effective discharge calculation: A practical guide. ERDC/CHL TR-00-15, U.S. Army Engineer Research and Development Center, Coastal and Hydraulics Laboratory.

Brown, C. B. (1950). *Sediment Transportation*. John Wiley & Sons Ltd., New York.

Crowder, D. W. and Knapp, H. V. (2005). Effective discharge recurrence intervals of Illinois streams. *Geomorphology*, 64(3-4):167 – 184.

Davis, B. E. (2005). The US DH-2: A one-liter hand-line isokinetic suspended-sediment/water-quality collapsible-bag sampler. Report SS, U.S. Geological Survey and the Federal Interagency Sedimentation Project, Vicksburg, MS.

Diplas, P., Kuhnle, R., Gray, J., Glysson, D., and Edwards, T. (2008). *Sedimentation Engineering: Processes, Measurements, Modeling, and Practice - Sediment Transport Measurements*, chapter 5, pages 307–353. ASCE Manuals and Reports on Engineering Practice No. 110. American Society of Civil Engineering.

Edwards, T. K. and Glysson, G. D. (1999). Field methods for measurement of fluvial sediment. Techniques of Water-Resources Investigations Book 3, Chapter C2, U.S. Geological Survey, Washington D.C.

Einstein, H. A. (1942). Formulas for the transport of bed load. *Transactions ASCE*, 107:561–573.

Emmett, W. and Wolman, M. (2001). Effective discharge and gravel-bed rivers. *Earth Surface Processes and Landforms*, 26(13):1369–1380.

Hey, R. D. (1997). Channel response and channel forming discharge: literature review and interpretation. Final Report U.S. Army Contract Number R&D 6871-EN-01.

Klonsky, L. and Vogel, R. M. (2011). Effective measures of “effective” discharge. *The Journal of Geology*, 119(1):1–14.

Lane, E. W. (1955). The importance of fluvial morphology in hydraulic engineering. *Journal of the Hydraulics Division, Proceedings of the ASCE*, 81(1):1–17.

Lenzi, M., Mao, L., and Comiti, F. (2006). Effective discharge for sediment transport in a mountain river: Computational approaches and geomorphic effectiveness. *Journal of Hydrology*, 326(1-4):257–276.

Ma, Y., Huang, H. Q., Xu, J., Brierley, G. J., and Yao, Z. (2010). Variability of effective discharge for suspended sediment transport in a large semi-arid river basin. *Journal of Hydrology*, 388(3-4):357 – 369.

Mackin, J. H. (1948). Concept of the graded river. *Geological Society of America Bulletin*, 59:463–512.

Meyer-Peter, E. and Müller, R. (1948). Formulas for bed-load transport. In *Proceedings of the Second Meeting*, pages 39–64, Stockholm, Sweden. IAHR.

Phillips, J. D. (2008). Geomorphic processes, controls,and transition zonesin the Middle and Lower Trinity River. Contract number 0704830781, Texas Water Development Board and Texas Instream Flow Program.

Pickup, G. and Warner, R. (1976). Effects of hydrologic regime on magnitude and frequency of dominant discharge. *Journal of Hydrology*, 29(1-2):51–75.

Rubey, W. W. (1933). Settling velocity of gravel, sand, and silt particles. *American Journal of Science*, 25(148):325–338.

Sichingabula, H. M. (1999). Magnitude-frequency characteristics of effective discharge for suspended sediment transport, fraser river, british columbia, canada. *Hydrological Processes*, 13(9):1361–1380.

Strom, K. and Rouhnia, M. (2013). Suspended sediment sampling and annual sediment yield on the lower brazos river. Final report, Texas Water Development Board.

Vogel, R. M., Stedinger, J. R., and Hooper, R. P. (2003). Discharge indices for water quality loads. *Water Resources Research*, 39(10):1273.

Whiting, P. J., Stamm, J. F., and Moog, D. B. (1999). Sediment-transporting flows in headwater streams. *Geological Society of America Bulletin*, 111(3):450–466.

Wolman, M. G. and Miller, J. C. (1960). Magnitude and frequency of forces in geomorphic processes. *Journal of Geology*, 68:54–74.

Wright, S. and Parker, G. (2004). Flow resistance and suspended load in sand-bed rivers: Simplified stratification model. *Journal of Hydraulic Engineering*, 130(8):796–805.